



Original Paper

Temperature- and alkali-resistant induced domestication of *Bacillus pasteurii* in drilling fluid and its borehole wall enhancement properties

Ze-Hua Du ^a, Zhi-Jun Li ^{a,*}, Jun-Xiu Chen ^b, Zi-Yi Ma ^a, Guang-Ding Guo ^a, Hao Zhang ^a, Sheng Wang ^a

^a State Key Laboratory of Geohazard Prevention and Geoenvironment Protection (Chengdu University of Technology), Chengdu University of Technology, Chengdu, 610059, Sichuan, China

^b China Water Resources Pearl River Planning, Surveying & Designing Co., Ltd, Guangzhou, 510000, Guangdong, China



ARTICLE INFO

Article history:

Received 2 April 2024

Received in revised form

25 July 2024

Accepted 24 September 2024

Available online 25 September 2024

Edited by Jia-Jia Fei and Teng Zhu

Keywords:

Broken formation

Instability of borehole wall

Bacillus pasteurii

Drilling fluid

Induced domestication

Wall enhancement properties

ABSTRACT

The microbial induced calcium carbonate precipitation (MICP) technology provides a new approach to solve borehole destabilization in broken formations; however, the high-temperature and alkaline environments inhibit the growth of microorganisms, which in turn affects the performance of their wall enhancement performance. In this study, a pH and temperature-coupled induced domestication method was applied to *Bacillus pasteurii*, and its wall enhancement performance was evaluated. Post domestication, *Bacillus pasteurii* exhibited high growth activity at pH 10.3 and temperature 45 °C. In a sodium carboxymethyl cellulose (CMC) drilling fluid environment, bacterial concentration reached 1.373 with urease activity at 1.98 after 24 h, and in a xanthan gum (XG) environment, the figures were 0.931 and 1.76, respectively—significantly higher than those before domestication. The *Bacillus pasteurii*-CMC system exhibited enhanced performance with the unconfined compressive strength of the specimen up to 1.232 MPa, permeability coefficient as low as 0.024, and calcium carbonate production up to 24.685 g. The crushed specimen portions remained lumpy with even calcium carbonate distribution. In contrast, the *Bacillus pasteurii*-XG system exhibited the highest unconfined compressive strength of 0.561 MPa, lowest permeability coefficient of 0.081, and the greatest calcium carbonate production of 16.03 g, with an externally cemented shell but internally loose structure and uneven calcium carbonate distribution, resulting in weaker mechanical properties. The *Bacillus pasteurii* induced predominantly vaterite calcium carbonate crystals in the CMC drilling fluid. In the XG drilling fluid, the crystals were mainly calcite. Both types effectively cemented the broken particles, improving formation strength and reducing permeability. However, under the same conditions, the *Bacillus pasteurii*-CMC system demonstrated a more pronounced enhancement effect.

© 2024 The Authors. Publishing services by Elsevier B.V. on behalf of KeAi Communications Co. Ltd. This is an open access article under the CC BY-NC-ND license (<http://creativecommons.org/licenses/by-nc-nd/4.0/>).

1. Introduction

In the fields of mineral resources exploration, development, and geotechnical engineering, encountering broken strata during drilling operations is inevitable. This often leads to serious destabilization of borehole walls, which can trigger drilling accidents such as jamming or buried drills. These incidents not only extend the drilling cycle but can also result in the scrapping of drilling

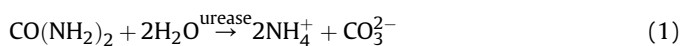
operations, leading to substantial economic losses (Qiu et al., 1999). Traditional wall protection measures typically involve the use of high-quality drilling fluid systems, casing, and grouting. A high-quality drilling fluid system is crucial for stabilizing the hole wall during drilling and is a preferred method among drilling engineers. However, in broken formations, the low cementation force between fractured blocks, combined with mechanical disturbances from drilling columns and bits, and the lubrication effect of drilling fluids penetrating the stratum, diminish the effectiveness of these wall protection measures (Tang and Luo, 1997; Qi and Ma, 2005). Casing, while effective in maintaining the wall of broken formations, can

* Corresponding author.

E-mail address: lizhijun2014@cdut.edu.cn (Z.-J. Li).

only be inserted post-hole formation. It is costly and complicates the hole structure (Niu et al., 2012). Grouting is effective for wall protection; however, the process is complex, quality control is challenging, and it poses a risk of polluting the geological environment (Wang, 2017). Consequently, a new drilling fluid system is urgently needed to address the problem of borehole wall destabilization in broken formations.

Both research and practical applications have demonstrated that enhancing the cementation force between fractured bodies and improving their inherent strength is a critical approach to resolving borehole wall destabilization in broken formations (Hu et al., 2011). Microbial induced calcium carbonate precipitation (MICP), based on microbial mineralization, has emerged as a prominent research area both domestically and internationally in recent years (Liu et al., 2019). MICP technology utilizes urease produced by microorganisms to catalyze the decomposition of urea, resulting in CO_3^{2-} production. This reacts with Ca^{2+} in the surroundings to form calcium carbonate precipitation, which exhibits cementation properties (Eq. (1) and Eq. (2)). MICP has been widely applied in soil consolidation, seepage reduction, and crack repair (Ivanov and Chu, 2008; Harkes et al., 2010; Phillips et al., 2016). Additionally, MICP technology offers the advantages of being environment friendly and cost-effective, providing a promising solution to the problem of borehole wall destabilization in broken formations.



Li et al. (2021a, 2022) have made significant advancements in the field of drilling fluid technology by integrating MICP into sodium carboxymethyl cellulose (CMC) cementless drilling fluid systems. Their core soaking experiments revealed that the microbial-CMC cementless drilling fluids could effectively cement and shape loose gravel soil, imparting it with a notable degree of unconfined compressive strength. They discovered that factors such as prolonged reaction time, increased concentration of cementing solution, and a higher initial bacterial strain concentration were beneficial for enhancing the gravel soil strength. Furthermore, Li et al. (2021b) observed that *Bacillus pasteurii* thrives in xanthan gum (XG) unconsolidated drilling fluids. However, their research did not account for the effects of ambient temperature and pH on the growth and wall enhancement performance of *Bacillus pasteurii* in these drilling fluid environments. In actual drilling operations, drilling fluids are typically alkaline (Liu et al., 2007), and borehole temperatures rise with increasing depth (Fu and Zhao, 2019). In the field of geological drilling, vast majority of wells are drilled to a depth of less than 2000 m, the temperature in the hole is generally below 60 °C, and the pH of solid-free drilling fluids are usually controlled at around 10.0, whereas for even shallower geological drilling wells, the temperature is usually less than 45 °C. These conditions are challenging for the metabolic activity of *Bacillus pasteurii*. Previous studies have demonstrated that temperature and pH are the main reasons affecting the MICP process (Sun et al., 2019a, 2019b; Wang et al., 2023a, 2023b), and that the metabolic activity of *Bacillus pasteurii* is markedly suppressed when the temperature is increased above 42 °C or the pH is high at 9.4 (Liu et al., 2019; Li et al., 2023a, 2023b), thus affecting its wall enhancing performance. The induced domestication strategy can significantly enhance the adaptability of organisms to their environment (Steensels et al., 2019). This technique could be utilized to acclimatize *Bacillus pasteurii* to high-temperature and strong alkaline conditions, thereby optimizing the MICP reaction and enhancing the wall reinforcement effect.

The induced domestication technique is a well-established method in diverse fields such as food, environment, and mining (Zhang et al., 2022; De Guidi et al., 2023; Zhang et al., 2023). This method has been instrumental in enhancing organism tolerance to various environmental conditions and facilitating their growth in new environments.

For instance, Wang (2022) employed a gradient domestication method to increase the tolerance of microalgae to high concentrations of CO_2 . By gradually raising the CO_2 concentration from 0.04% to 12%, Wang successfully developed *Micrococcus* sp. strains capable of tolerating a high concentration of 15% CO_2 . This study validated the efficacy of CO_2 gradient domestication as a stable and effective approach for cultivating microalgal strains that can withstand high CO_2 concentrations.

Tang et al. (2012) applied domestication techniques to adapt the fermenting strain of lactic acid bacteria in sour soy milk. By gradually increasing the proportion of soy milk in cow milk using passaging domestication and adding soy peptide digest, they enhanced the bacteria's adaptation to the soy-milk environment and its vitality. Their study demonstrated that these domestication methods positively affect the growth of lactic acid bacteria in sour soy milk, improving their tolerance and maintaining or even enhancing their activity levels. Cui et al. (2019) conducted a six-month copper tolerance directed domestication of *Acidithiobacillus caldus*. The resulting strain exhibited strong resistance to copper stress and maintained an active biochemical leaching effect in the leaching system post-domestication. Similarly, Zheng et al. (2019) used a continuous transfer domestication method to develop arsenic tolerance in *Leptospirillum ferriphilum*, a moderately thermophilic acidophilic leaching bacterium. The domesticated strain exhibited significantly increased arsenic tolerance and an optimized leaching effect on arsenopyrite. In addition to metal tolerance, domestication has proven effective in adapting organisms to external temperature and pH changes. Wang et al. (2022) subjected fish ZF4 cells to short-term low-temperature stress and long-term low-temperature domestication, discovering that this process enhanced the cells' low-temperature tolerance. Li et al. (2016) improved the acid and oxygen tolerance of *Lactobacillus paracasei* L9 through domestication under low pH and high oxygen concentration stress. The domesticated strain exhibited high β -galactosidase gene expression, strong enzyme activity, robust acid production capacity, and stability during storage. The domestication technology has also been applied in the realm of MICP; Xiao et al. (2022) performed multi-gradient domestication of *Bacillus pasteurii* in an artificial seawater environment. The domesticated bacteria showed improved adaptability to seawater and enhanced MICP performance. Therefore, employing induced domestication to adapt *Bacillus pasteurii* to drilling fluid environments with high alkalinity and then improving its temperature tolerance is crucial. This approach is necessary to enhance the wall-strengthening ability of *Bacillus pasteurii* under high-temperature and strongly alkaline conditions, a key factor for the successful application of MICP technology in maintaining borehole wall stability in broken formations.

In summary, this study aimed to ensure the high growth activity and efficient MICP wall-enhancing capability of *Bacillus pasteurii* under drilling fluid environments with elevated pH and temperature. To achieve this, the study focused on the pH and temperature-coupled induction domestication of *Bacillus pasteurii* within the drilling fluid system. Key influencing factors, such as initial bacterial concentration, cementing solution concentration, temperature, and action time, were identified to design orthogonal experiments for MICP wall consolidation. These experiments measured the physico-mechanical strength, permeability coefficient, and calcium carbonate production of the specimens post-wall consolidation,

providing a comprehensive evaluation of the wall enhancement performance of *Bacillus pasteurii* following induced domestication. Additionally, analytical techniques such as X-ray diffraction (XRD) and scanning electron microscopy (SEM) were employed to investigate the material composition and microstructure of the specimens, both before and after the wall enhancement experiments. These analyses were crucial in understanding the reasons behind the varying wall enhancement effects observed in *Bacillus pasteurii*, both in its induced and domesticated forms, across different drilling fluid systems. The findings of these experiments and analyses are expected to significantly contribute to the field, offering insights into optimizing MICP technology for enhanced borehole stability in challenging drilling environments.

2. Materials and methods

2.1. Materials

The experimental study utilized quartz-based sand as gravel soil, which was meticulously cleaned, dried, and sieved. The soil demonstrated specific granulometric characteristics: D_{60} was measured at 0.65, D_{30} at 0.19, and D_{10} at 0.093. The coefficient of homogeneity (C_u) was calculated to be 6.99, and the coefficient of curvature (C_c) was determined to be 0.60. These parameters indicated that the soil was poorly graded. The grading curves of the soil are depicted in Fig. 1, and additional parameters are detailed in Table 1. The rest of the materials used in the experiment are listed in Table 2.

2.2. Methods

2.2.1. Bacterial liquid preparation

For the cultivation of *Bacillus pasteurii*, a strain sourced from Beijing Biotech Co., Ltd. (China), specifically No. ATCC-11859, was utilized. The preparation of the liquid culture medium involved adding 5 g of soy peptone, 15 g of casein peptone, 5 g of NaCl, and 20 g of urea to 1000 mL of deionized water. The pH of this mixture was adjusted to 7.3 using NaOH solution. This solution was then autoclaved at 121 °C under a pressure of 0.1 MPa for 20 min using an autoclave from Shanghai Bo Xun Industry Co. Ltd. (model YXQ-SG46-280S). Post-autoclaving, the medium was cooled to room temperature on a sterile operating table provided by Suzhou Antai

Air Technology Co., Ltd. (model SW-CJ1FD). After cooling, the activated *Bacillus pasteurii* organisms were inoculated into the medium. The mouth of the conical flask containing the culture was sterilized with an alcohol lamp and sealed with medical gauze. Subsequently, the flask was placed in a constant temperature incubator from Shanghai Zhichu Instrument Co., Ltd. (model ZHTY-50s). The culture was then incubated for 24 h at 30 °C and a shaking speed of 120 rpm. This process resulted in the bacterial liquid that was used in the experimental study.

2.2.2. Determination of bacteria concentration and urease activity

2.2.2.1. Determination of bacteria concentration. The concentration of bacteria in this study was quantified using the turbidimetric method, which involves measuring the absorbance of the bacterial liquid. For this purpose, a sample of the bacterial liquid was analyzed using an ultraviolet spectrophotometer (Shanghai Right One Instrument Co., Ltd., UV2000). The absorbance was measured at a wavelength of 600 nm (OD_{600}), and the resulting value was used to represent the concentration of the bacterial cells.

2.2.2.2. Determination of urease activity. The urease activity of the bacterial solution was achieved by mixing the bacterial solution with a 1.6 mol/L urea solution in a V/V ratio of 1:9. The change in conductivity of this mixed solution was measured at room temperature over a period of 5 min using a conductivity meter (Shanghai LeiMagnet Chuangyi Instrument Table Co., Ltd., DDS-11A). The average change in conductivity per minute (ms/min) was then calculated. According to Whiffin (2004), a conductivity change of 1 ms/min is equivalent to the hydrolysis of 11 mM of urea per minute. Therefore, the amount of urea hydrolyzed per minute by the bacterial solution (expressed in mM urea hydrolyzed \cdot min⁻¹) can be calculated by multiplying the observed conductivity change by the dilution factor of 10. In this study, the urease activity of the bacterial solution was expressed and calculated using this method.

$$\text{Urease activity (mM urea hydrolysed} \cdot \text{min}^{-1}) = \frac{\text{Conductivity change value} \times 11 \times 10}{5} \quad (3)$$

2.2.3. Preparation of drilling fluids

Li et al. (2023b) demonstrated that CMC and XG are suitable drilling fluid materials for configuring microbial drilling fluids; therefore, CMC and XG were chosen to configure microbial drilling fluids; the configuration is detailed below.

In the preparation of the drilling fluids for the experiment, CMC and an XG were used as additives to the liquid medium. Initially, 8 g of CMC was added to the liquid medium. This mixture was thoroughly blended using a high-speed blender. The pH of the drilling fluid was then adjusted to 7.3 using a 1 mol/L NaOH solution. Subsequently, the mixture was sterilized in a high-temperature steam sterilization kettle at 121 °C and 0.1 MPa for 20 min. After sterilization, the fluid was cooled to room temperature on a sterile operating table. This process resulted in the formation of a 0.8% CMC solid-free drilling fluid, henceforth referred to as Drilling Fluid P. Similarly, for the preparation of Drilling Fluid Q, 3 g of the XG was added to the liquid medium. Following the same procedure as above, a 0.3% XG solid-free drilling fluid was configured.

To introduce *Bacillus pasteurii* into these drilling fluids, 15 mL of the bacterial solution was inoculated into 150 mL of both drilling fluid P and Q, using a sterile pipette gun. These mixtures were then placed in a constant temperature oscillating incubator at 30 °C and 120 rpm for 24 h. This process yielded two types of microbial

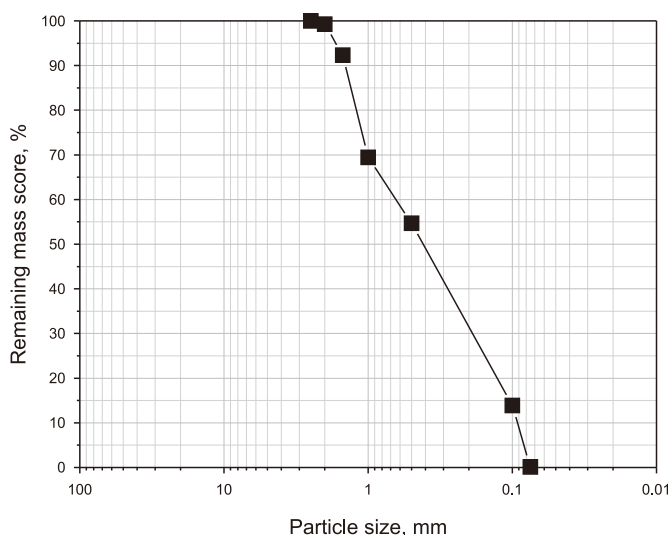


Fig. 1. Gradation curve for gravel soil particles.

Table 1
Grain size distribution and percentage content of sand.

Size, mm	>2.5	2.5–2.0	2.0–1.5	1.5–1.0	1.0–0.5	0.5–0.1	<0.1
Sieve mass, g	8.75	83.11	274.62	177.22	489.3	165.4	1.60
percentage content, %	0.73	6.92	22.89	14.77	40.78	13.78	0.13

Table 2
Other materials used in the experiment.

Material	Source of purchase	Specification
Deionized water	Chengdu Kelong Electronics Co., Ltd., China.	
Casein peptone, Soy peptone	Beijing Soleibao Technology Co., Ltd., China.	Biological reagents
XG	Shandong Shenghuang Chemical Products Co., Ltd., China	
CMC	Sinopharm Group Chemical Reagent Co., Ltd., China.	Chemically pure
NaCl	Fortune (Tianjin) Chemical Reagent Co., Ltd., China.	Chemically pure
Urea	Sinopharm Group Chemical Reagent Co., Ltd., China.	Chemically pure
NaOH	Sinopharm Group Chemical Reagent Co., Ltd., China.	Chemically pure
CaCl ₂	Sinopharm Group Chemical Reagent Co., Ltd., China.	Chemically pure
HCl	Chengdu Kelong Electronics Co., Ltd., China.	Chemically pure
Geotextile		

drilling fluids: *Bacillus pasteurii*-CMC drilling fluid and *Bacillus pasteurii*-XG drilling fluid. After 24 h of incubation, the OD₆₀₀ values for the *Bacillus pasteurii*-CMC and *Bacillus pasteurii*-XG drilling fluids were measured to be 3.71 and 2.551, respectively. Additionally, the urease activities for both fluids were recorded at 4.4 mM urea hydrolyzed per minute. The properties of the 0.8% CMC unsolidified drilling fluid, 0.3% XG unsolidified drilling fluid, *Bacillus pasteurii*-CMC drilling fluid after 24 h of incubation, and *Bacillus pasteurii*-XG drilling fluid after 24 h of incubation are detailed in Table 3.

2.2.4. Alkali-and temperature-tolerant coupled domestication of *Bacillus pasteurii*

The coupled domestication of *Bacillus pasteurii* in drilling fluids P and Q environments, characterized by specific pH and temperature conditions, is achieved through two distinct methods: direct domestication and gradient domestication. For this purpose, *Bacillus pasteurii*, cultured at a pH of 7.3, temperature of 30 °C, and rotational speed of 120 rpm, serves as the seed organism. Each experimental group is subjected to three parallel experiments to ensure reliability, with the results subsequently averaged for precision. The domestication method is illustrated in Fig. 2.

2.2.4.1. Direct domestication

a. pH direct domestication

The pH of drilling fluids P and Q is adjusted to the target pH of 10.3 for domestication. Subsequently, the seed bacteria are inoculated into these fluids (maintaining a volume ratio of bacterial fluid to liquid medium at 1:10). The bacteria are then incubated for 24 h at 30 °C and 120 rpm. Optical density at 600 nm (OD₆₀₀) and urease activity are measured at the 24th hour. Following this, the culture is expanded multiple times until OD₆₀₀ stabilizes, resulting in the

acquisition of *Bacillus pasteurii* x, which has been directly domesticated in a strong alkali environment. OD₆₀₀ and urease activity are recorded at the 24th hour post-stabilization for both the initial and expansion cultures, the same for part b.

b. pH, temperature coupled direct domestication

The procedure begins by adjusting the pH of drilling fluids P and Q to 10.3, followed by the inoculation of *Bacillus pasteurii* x. The culture is incubated for 24 h at the domestication target temperature of 45 °C and a rotational speed of 120 rpm. OD₆₀₀ and urease activity measurements are taken at the 24th hour. The culture is then expanded several times until OD₆₀₀ stabilization, resulting in the production of *Bacillus pasteurii* y, which is directly domesticated under coupled alkali and temperature conditions.

2.2.4.2. Gradient domestication

a. pH gradient domestication

Five pH gradients are established, ranging from the optimal growth pH of 7.3 to the domestication target pH of 10.3: 8.3, 8.8, 9.3, 9.8, and 10.3. The pH of drilling fluids P and Q is initially adjusted to 8.3. Subsequently, the seed organisms into these fluids are inoculated and incubated at 30 °C and 120 rpm for a duration of 24 h. Subsequently, multiple rounds of expansion culture are conducted until OD₆₀₀ demonstrates a trend toward stabilization after 24 h. This process results in the gradient domestication of *Bacillus pasteurii* X_{8.3}. In a similar manner, adjusting the pH of drilling fluids P and Q to 8.8, inoculating with *Bacillus pasteurii* X_{8.3}, and incubating under the same conditions results in the cultivation of *Bacillus pasteurii* X_{8.8}. Multiple rounds of expansion culture are again conducted until the OD₆₀₀ stabilizes at the 24 h mark. Following this protocol iteratively finally affords *Bacillus pasteurii* X_{10.3}. OD₆₀₀ and

Table 3
Drilling fluid properties.

Drilling fluid	Density, g	Funnel viscosity, s	Apparent viscosity, mPa·s	Plastic viscosity, mPa·s	Dynamic shear, Pa
0.8% CMC	1.01	100.21	50.5	29.5	21
0.3% XG	1.01	29.17	14.25	6.5	7.75
<i>Bacillus pasteurii</i> -CMC	1.01	23.78	10.5	5.5	5
<i>Bacillus pasteurii</i> -XG	1.01	22.03	11.5	5	6.5

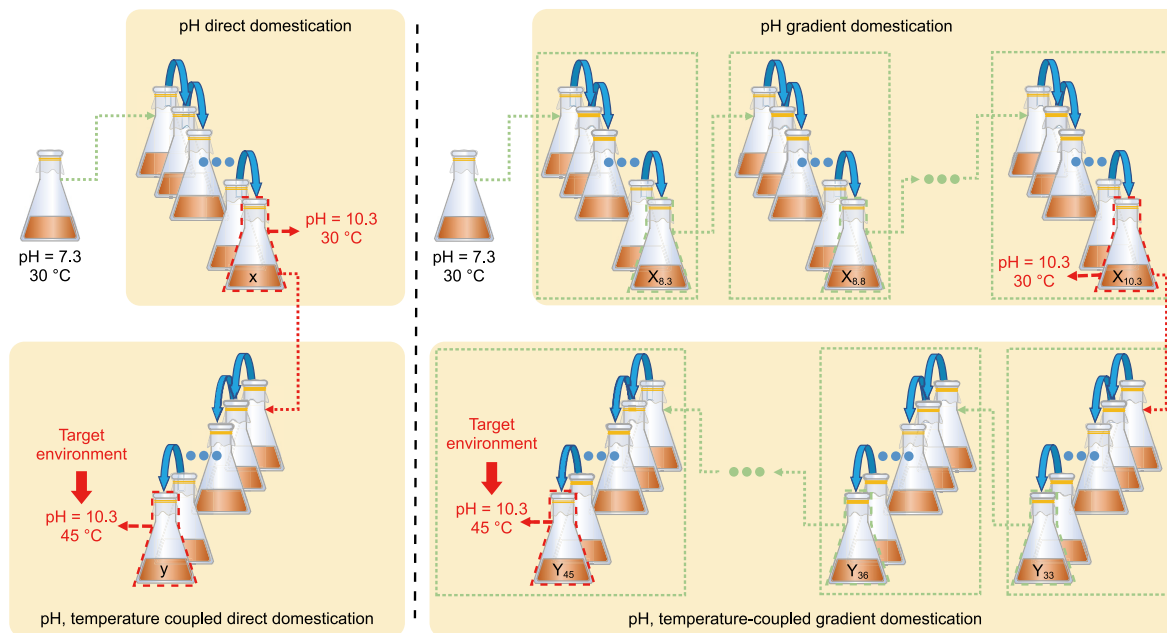


Fig. 2. Illustration of the domestication method.

urease activity are recorded at the 24th hour post-stabilization for both the initial and expanded cultures at each pH gradient, the same for part b.

b. pH, temperature-coupled gradient domestication

Five temperature gradients are set between the optimal growth temperature of 30 °C and the domestication target temperature of 45 °C: 33, 36, 39, 42, and 45 °C. The pH of drilling fluids P and Q is adjusted to 10.3, and *Bacillus pasteurii* X_{10.3} is inoculated and incubated at 33 °C, 120 rpm for 24 h. Post-incubation, the culture undergoes several expansions until the OD₆₀₀ stabilizes at the 24th hour, resulting in *Bacillus pasteurii* Y₃₃. Y₃₃ is inoculated into new drilling fluids P and Q with pH 10.3, and incubated at 36 °C and 120 rpm for 24 h. Subsequently, the culture is repeatedly expanded until the OD₆₀₀ stabilizes at the 24th hour, resulting in the derivation of *Bacillus pasteurii* Y₃₆. This process eventually leads to the attainment of *Bacillus pasteurii* Y₄₅.

2.2.5. Microbial drilling fluid borehole wall enhancement experiment

2.2.5.1. Borehole wall enhancement experiment.

The *Bacillus pasteurii* wall enhancement experiment is conducted using the core immersion method. The experimental setup includes a beaker, PVC bracket, metal mold, geotextile flexible mold, and magnetic stirrer, as illustrated in Fig. 3. The fiber structure of the geotextile can provide support to the originally loose specimen. Simultaneously, the existence of a large number of pores between the fibers gives it good permeability, and the *Bacillus pasteurii*-drilling fluid can significantly enter the interior of the specimen to carry out the MICP reaction, minimizing the influence of the mold on the experimental results. The specific experimental methods are described as follows:

Firstly, 2 L of *Bacillus pasteurii*-drilling fluid is prepared, with the bacterial concentration adjusted to the predetermined value. The experimentally determined quantities of CaCl₂ and CO(NH₂)₂ are added and thoroughly mixed. Subsequently, the geotextile is cut and fashioned into a cylindrical mold with dimensions of 50 mm in

height and diameter, as shown in Fig. 4. Gravel soil samples weighing 150 g are prepared by soaking them in 0.1 mol/L HCl solution for 24 h prior to the experiment, followed by washing and drying with deionized water. These samples are then gradually loaded into the flexible molds, ensuring full contact, and gently compacted into a specimen.

The beaker is placed on a magnetic stirrer, and the rotor and PVC bracket are positioned inside it. The specimen is placed in a metal container on the PVC bracket. Following this, all the *Bacillus pasteurii*-drilling fluid is poured into the beaker. The heating and stirring functions of the magnetic stirrer are activated, set to the desired temperature, and appropriate rotational speed. Control groups using drilling fluids P and Q are set up in a similar manner.

After the predetermined time for the wall enhancement experiment, the specimens are removed from the experimental setup and immersed in deionized water. This step is crucial for gently removing soluble impurities and soft calcium carbonate deposits from the surface. The specimens are then dried at 80 °C for 12 h. At the end of the drying period, the molds are carefully disassembled, and the obtained specimens are prepared for subsequent tests.

To elucidate the impact of wall enhancement by *Bacillus pasteurii* following its domestication under coupled gradients of pH and temperature, MICP wall enhancement orthogonal experiments are conducted. These experiments aim to determine key parameters of the specimens post wall-enhancement, specifically unconfined compressive strength, permeability coefficient, and calcium carbonate production. The experimental variables are initial bacterial concentration (A), cementing solution concentration (B), temperature (C), and time (D). The orthogonal experimental design adopts a four-factor, five-level approach, as outlined in Table 4. The orthogonal table L₂₅ (4⁵) from IBM SPSS Statistics software is utilized for this design and is detailed in Table 5. Notably, the empty columns in this table serve a dual purpose: they estimate experimental error and measure the reliability of the experiment. Additionally, they facilitate the analysis of each factor's influence on wall enhancement performance through range analysis. A comprehensive series of 25 distinct experimental groups is conducted within

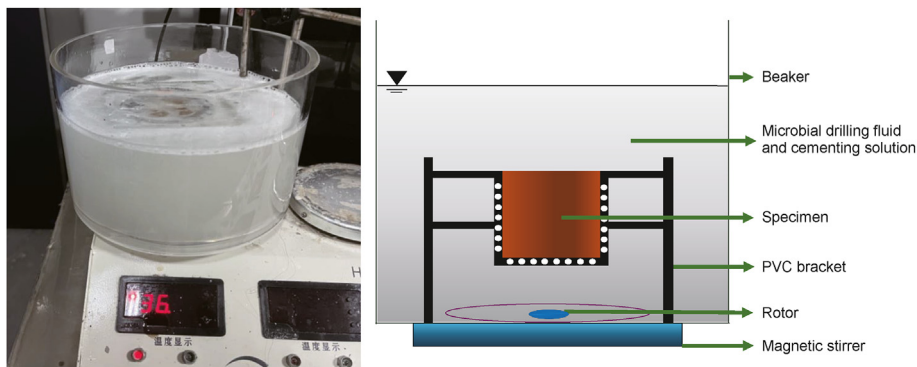


Fig. 3. Experimental setup of the MICP wall enhancement experiment.

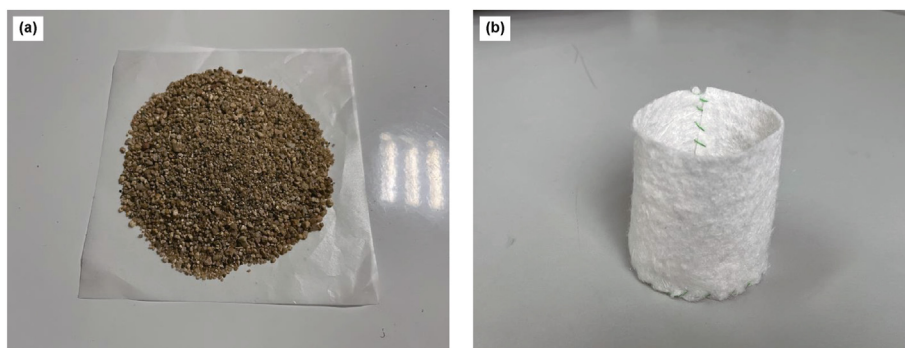


Fig. 4. Gravel soil and full-contact flexible mold ((a) gravel soil; (b) full-contact flexible mold).

Table 4
Table of factor levels of orthogonal experimental program.

Level	Factor			
	A	B	C	D
	OD ₆₀₀	mol/L	°C	h
1	0.3	0.2	33	12
2	0.6	0.4	36	24
3	0.9	0.6	39	36
4	1.2	0.8	42	48
5	1.5	1.0	45	60

this orthogonal framework. To ensure accuracy and repeatability, each group undergoes three iterations, with the resultant data averaged for analysis. This methodical approach ensures a robust examination of the variables impacting the wall enhancement efficacy of *Bacillus pasteurii*.

2.2.5.2. *Unconfined compression test.* In this experiment, the CDUT-ZJ01 unconfined compressive tester, jointly developed by Chengdu University of Technology and Jiangsu Kedi Petroleum Instrument Co., Ltd., China, is employed. Upon completion of the MICP wall enhancement experiment, the specimen is positioned at the center axis of the lifting table of the testing machine for the unconfined compressive strength test. The loading rate for the specimen is set to 0.05 mm/min, continuing until specimen failure. During the test, the computer-controlled universal testing machine automatically records the pressure value F , the duration of the experiment, and the stress-time variation curve. For each set of experiments, three parallel tests are conducted, and their average value is calculated.

The formula for calculating the unconfined compressive

strength R_c of the specimen is as follows:

$$R_c = \frac{F}{A}, \tag{4}$$

where

- R_c : Unconfined compressive strength of the specimen, MPa;
- F : Aximum pressure at destruction of the specimen, N;
- A : Contact area of the specimen with the pressure plate, mm².

2.2.5.3. *Penetration test.* The permeability coefficient of the specimen, both pre- and post-curing, is determined using the constant head method. The experimental apparatus for measuring the permeability coefficient is designed in accordance with Darcy's law (Wang et al., 2015; Sun et al., 2021), as depicted in Fig. 5. To ensure that water flows through the interior of the specimen from top to bottom while maintaining a constant head, the gap between the specimen and the PVC pipe is sealed with a sealant. The permeability coefficient is calculated using Eq. (5), based on Darcy's law of percolation, as follows:

$$K = \frac{QL}{Aht}, \tag{5}$$

where

- K : Permeability coefficient, md;
- Q : Penetration volume, mL;
- A : Cross-sectional area of the water, cm²;
- H : Height of the water head, cm;

Table 5
Table of orthogonal experimental design.

Number	A, OD ₆₀₀	B, mol/L	C, °C	D, h	Empty column 1	Empty column 2
1	1 (0.3)	1 (0.2)	1 (33)	1 (12)	1	1
2	1 (0.3)	2 (0.4)	3 (39)	4 (48)	5	2
3	1 (0.3)	3 (0.6)	5 (45)	2 (24)	4	3
4	1 (0.3)	4 (0.8)	2 (36)	5 (60)	3	4
5	1 (0.3)	5 (1.0)	4 (42)	3 (36)	2	5
6	2 (0.6)	1 (0.2)	5 (45)	4 (48)	3	5
7	2 (0.6)	2 (0.4)	2 (36)	2 (24)	2	1
8	2 (0.6)	3 (0.6)	4 (42)	5 (60)	1	2
9	2 (0.6)	4 (0.8)	1 (33)	3 (36)	5	3
10	2 (0.6)	5 (1.0)	3 (39)	1 (12)	4	4
11	3 (0.9)	1 (0.2)	4 (42)	2 (24)	5	4
12	3 (0.9)	2 (0.4)	1 (33)	5 (60)	4	5
13	3 (0.9)	3 (0.6)	3 (39)	3 (36)	3	1
14	3 (0.9)	4 (0.8)	5 (45)	1 (12)	2	2
15	3 (0.9)	5 (1.0)	2 (36)	4 (48)	1	3
16	4 (1.2)	1 (0.2)	3 (39)	5 (60)	2	3
17	4 (1.2)	2 (0.4)	5 (45)	3 (36)	1	4
18	4 (1.2)	3 (0.6)	2 (36)	1 (12)	5	5
19	4 (1.2)	4 (0.8)	4 (42)	4 (48)	4	1
20	4 (1.2)	5 (1.0)	1 (33)	2 (24)	3	2
21	5 (1.5)	1 (0.2)	2 (36)	3 (36)	4	2
22	5 (1.5)	2 (0.4)	4 (42)	1 (12)	3	3
23	5 (1.5)	3 (0.6)	1 (33)	4 (48)	2	4
24	5 (1.5)	4 (0.8)	3 (39)	2 (24)	1	5
25	5 (1.5)	5 (1.0)	5 (45)	5 (60)	5	1

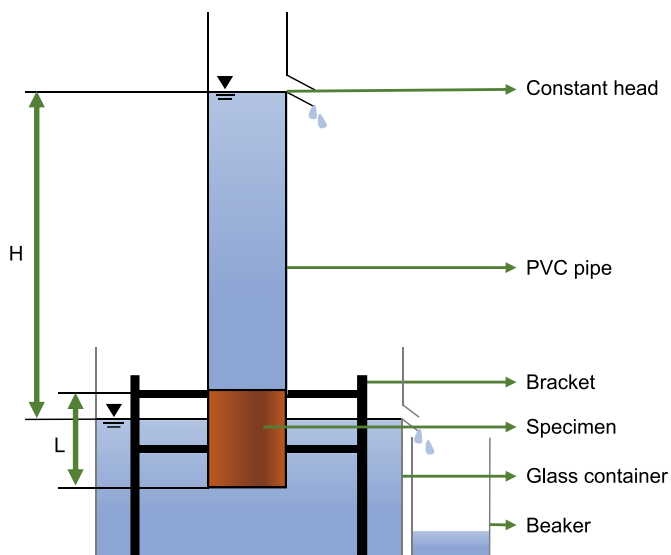


Fig. 5. Diagram of the experimental device for the determination of permeability coefficient.

L: Length of the penetration path, that is, the height of the specimen, cm;
t: Given time interval, s.

2.2.5.4. Measurement of calcium carbonate production. The determination of calcium carbonate production in the specimen is conducted using hydrochloric acid titration. Initially, the specimen's mass post-experimentation is measured and recorded as *M*₁. The specimen is then immersed in an excess of 0.1 mol/L HCl solution to ensure complete reaction, indicated by the cessation of bubble formation. Following this, the specimen is filtered through filter paper and rinsed several times with deionized water. Subsequently, it is placed back in the oven for drying and then weighed again,

with this weight recorded as *M*₂. The amount of calcium carbonate (*M*) produced as a result of the MICP action in the specimen is calculated based on the difference in mass between these two measurements (*M*₁ and *M*₂) as follows:

$$M = M_1 - M_2. \tag{6}$$

Similarly hydrochloric acid titration experiments are conducted on pure gravel soil samples, drilling fluid P group, drilling fluid Q group, *Bacillus pasteurii*-CMC drilling fluid group, and *Bacillus pasteurii*-XG drilling fluid group to observe the changes.

2.2.6. Microanalytical experiments

For further analysis, XRD is utilized to characterize the specimens from pure gravel soil samples, drilling fluid group, and *Bacillus pasteurii*-drilling fluid group. The XRD analysis involves setting the scanning range from 5° to 70° and adjusting the scanning speed to 0.02°/step. The X-ray diffraction peak profiles of the obtained specimens are then compared with the diffraction peak profiles of standard PDF cards to analyze the primary components present in each group of specimens. Additionally, the microstructures of the pure gravel soil samples, drilling fluid group, and *Bacillus pasteurii*-drilling fluid group specimens are examined using SEM to gain insight into the microstructural characteristics of the specimens.

3. Results and discussion

3.1. Alkali- and temperature-tolerant coupled domestication of *Bacillus pasteurii*

The concentration and urease activity of *Bacillus pasteurii* in direct domestication, and the first incubation under each domestication gradient and at the 24th hour post domestication stabilization are depicted in Figs. 6 and 7.

Figs. 6 and 7 illustrate that in the process of pH and temperature-coupled induced domestication, the gradient domestication approach is more effective for *Bacillus pasteurii* than direct domestication. This is evidenced by higher bacterial

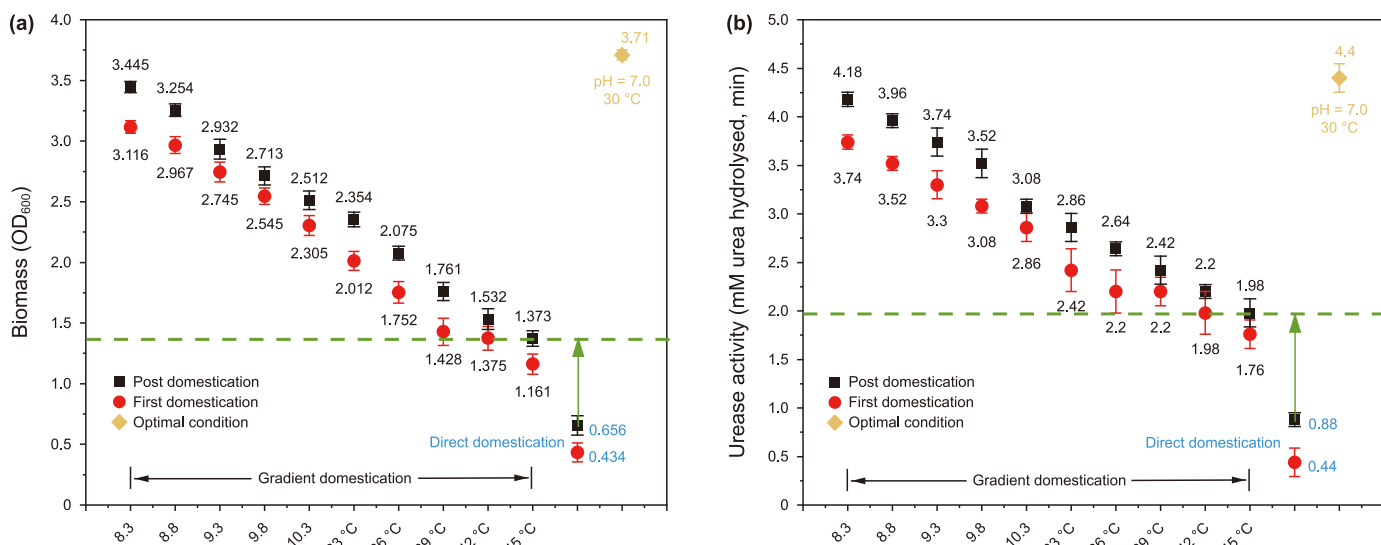


Fig. 6. Changes in bacterial concentration and urease activity of *Bacillus pasteurii* after induced domestication in drilling fluid P ((a) bacterial concentration; (b) urease activity).

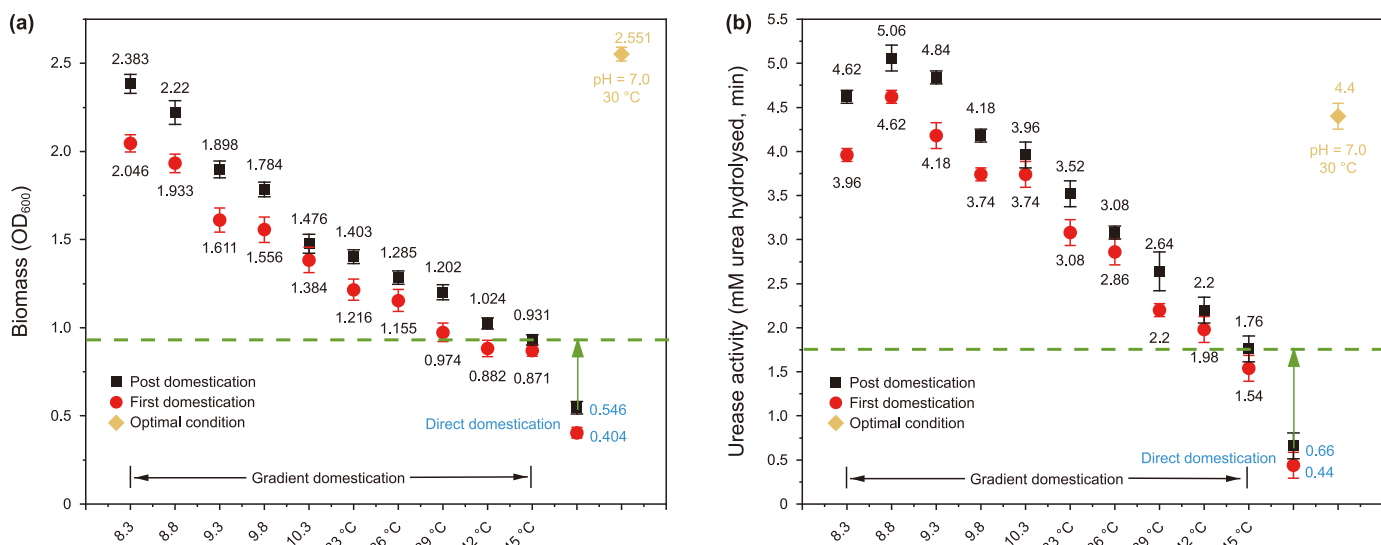


Fig. 7. Changes in bacterial concentration and urease activity of *Bacillus pasteurii* after induced domestication in drilling fluid Q ((a) bacterial concentration; (b) urease activity).

concentrations and urease activity at the 24th h, as well as after several expanded cultures to reach stability, compared with the initial culture. Under direct domestication, *Bacillus pasteurii* exhibits lower bacterial concentration and urease activity, with minimal enhancement after repeated expanded cultures. This suggests that strong alkali and higher temperatures significantly inhibit the growth and reproduction of *Bacillus pasteurii*.

In the drilling fluid Q domestication environment, the urease activity of *Bacillus pasteurii* increases with pH in the 8.3–9.3 range but decreases in the 9.3–10.3 range. This is because *Bacillus pasteurii*, a moderately alkalophilic bacterium (Zhang et al., 2023), experiences increased cell-membrane permeability within the 8.3–9.3 pH range, facilitating nutrient and metabolite exchange between the inside and outside of the cell and reducing intracellular toxic product inhibition, thereby enhancing metabolism (Pei et al., 2020). However, beyond pH 9.3, rising pH levels gradually damage the cell-membrane integrity, inhibiting metabolism and potentially causing cell death.

In drilling fluids P and Q environments, *Bacillus pasteurii* Y₄₅,

obtained through gradient domestication, exhibits concentrations of 1.373 and 0.931, with urease activities of 1.98 and 1.76 at the 24th h, respectively. These values are significantly higher than those obtained through direct domestication. This indicates that gradient domestication enables *Bacillus pasteurii* to better adapt to environmental pH and temperature changes, demonstrating enhanced growth activity. This adaptation is attributed to the gradual transition from favorable to extreme environments under gradient domestication, leading to increased total lipid and high melting point saturated fatty acid content in the cell membrane. This improves the strain's alkali and heat resistance (Zhang et al., 2019), possibly alongside increased FOF1-ATPase enzyme expression, enhancing pH stability across the cell membrane and improving alkali resistance (Kobayashi et al., 1986; Krulwich et al., 2011; Zhang et al., 2019). However, direct domestication in more extreme environments does not effectively enhance the adaptation capabilities of *Bacillus pasteurii*. Instead, it leads to spore dormancy or death (He et al., 2023), resulting in less effective domestication compared to gradient domestication.

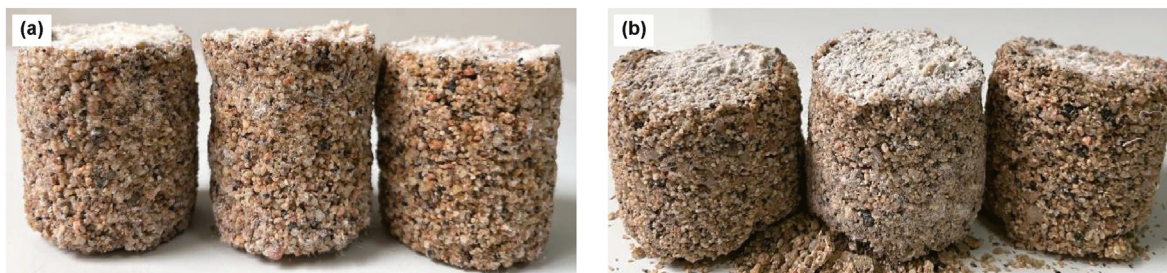


Fig. 8. Specimens after MICP orthogonal wall enhancement experiments ((a) *Bacillus pasteurii*-CMC drilling fluid group; (b) *Bacillus pasteurii*-XG drilling fluid group).

3.2. Microbial borehole wall enhancement experiment

Fig. 8 displays the specimen shaped post the *Bacillus pasteurii* MICP wall enhancement orthogonal experiment, revealing that loose gravel soil particles are cemented into a solid cylindrical form. Fig. 9 depicts the damage to these specimens following the unconfined compressive test. In the *Bacillus pasteurii*-CMC drilling fluid group, damage occurs internally along the cylinder's top, forming block-shaped fragments. Conversely, in the *Bacillus pasteurii*-XG drilling fluid group, damage manifests along the surface, resulting in flake-like cementation with a loosely flaked interior. However, the specimens of drilling fluid groups P and Q were not cemented and remained loose. The stress-time curve of the

specimen exhibiting the highest unconfined compressive strength is presented in Fig. 10. Here, the stress escalates with time until the specimen's damage point, beyond which stress rapidly declines. The peak stress value represents the specimen's maximum unconfined compressive strength. Table 6 summarizes the unconfined compressive strength, permeability coefficient, and calcium carbonate production for each specimen in the wall enhancement orthogonal experimental program.

Table 6 illustrates the results of 25 groups in the *Bacillus pasteurii*-CMC drilling fluid wall enhancement orthogonal experiment. Among these, 24 groups formed specimens with discernible mechanical strength. The highest unconfined compressive strength recorded was 1.232 MPa, the lowest permeability coefficient was



Fig. 9. Diagram of the unconfined compression experiment specimens ((a) unconfined compression experiment; (b) specimen damage in the unconfined compression experiment of *Bacillus pasteurii*-CMC drilling fluid group; (c) specimen damage of the unconfined compression experiment of *Bacillus pasteurii*-XG drilling fluid group).

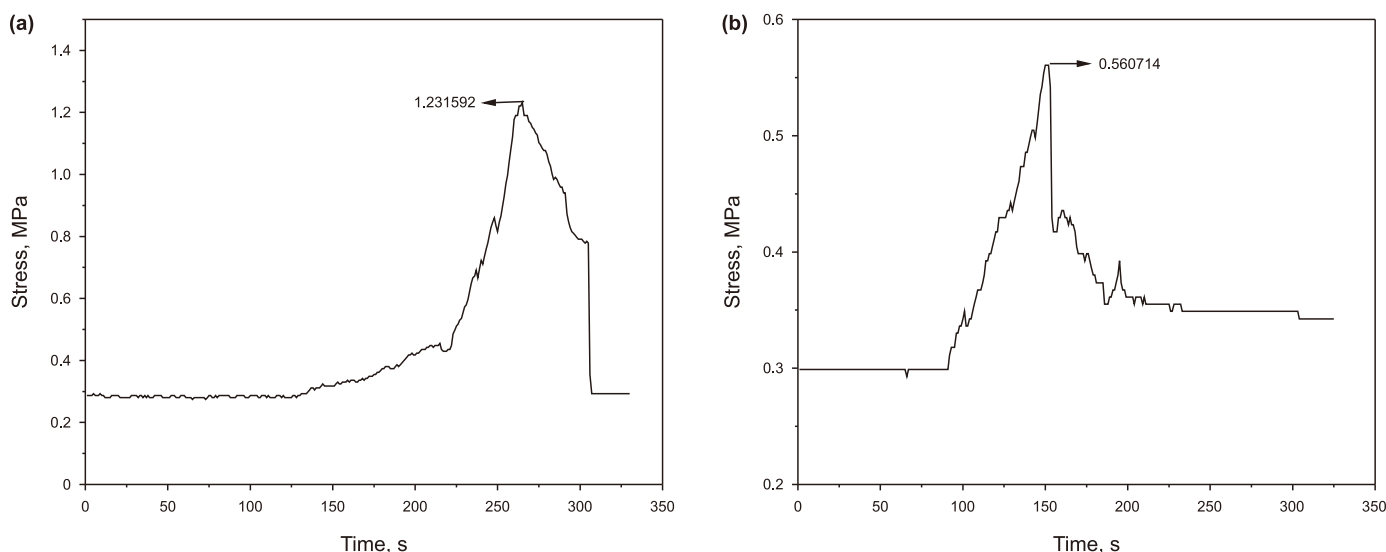


Fig. 10. Stress-time curves of specimen of the unconfined compression experiments ((a) *Bacillus pasteurii*-CMC drilling fluid group; (b) *Bacillus pasteurii*-XG drilling fluid group).

Table 6
Results of orthogonal experiments.

Number	Unconfined compressive strength, MPa		Permeability coefficient, md		Calcium carbonate production, g	
	CMC	XG	CMC	XG	CMC	XG
	1	/	/	0.150910	0.261314	2.35
2	0.448469	0.315646	0.106621	0.219856	7.33	6.48
3	0.320255	/	0.093350	0.231672	7.96	5.49
4	0.501224	0.305102	0.052657	0.180045	8.86	7.32
5	0.361224	/	0.080221	0.207609	10.67	3.28
6	0.357707	0.286735	0.094623	0.214623	3.63	2.94
7	0.531720	/	0.067943	0.237795	6.75	5.10
8	0.827516	0.390306	0.024365	0.123445	11.78	9.09
9	0.622704	0.460127	0.056617	0.176886	16.55	12.14
10	0.485096	/	0.096453	0.249319	7.66	6.97
11	0.314140	/	0.129503	0.242737	5.87	5.44
12	0.604082	0.460714	0.040643	0.156708	23.45	14.77
13	0.777580	0.454592	0.049331	0.171057	6.46	5.71
14	0.724586	0.286735	0.057616	0.204549	5.69	4.88
15	0.853231	0.522293	0.039173	0.138253	18.63	12.16
16	0.635204	0.385350	0.070440	0.197829	9.65	5.05
17	0.699618	0.348535	0.046556	0.159791	11.27	7.54
18	0.516433	0.323567	0.061111	0.198316	7.74	2.77
19	1.033929	0.454592	0.025580	0.121829	14.53	8.79
20	0.410701	0.382803	0.080320	0.185062	14.78	13.97
21	0.389286	0.292484	0.084031	0.211420	10.89	7.28
22	0.510064	0.323567	0.062865	0.170437	8.70	4.27
23	1.065051	0.497834	0.031536	0.110800	16.82	14.18
24	0.786752	0.444898	0.040811	0.156045	12.61	8.22
25	1.231592	0.560714	0.024006	0.080623	24.69	16.03

Note: “/” indicates that the specimen is unformed.

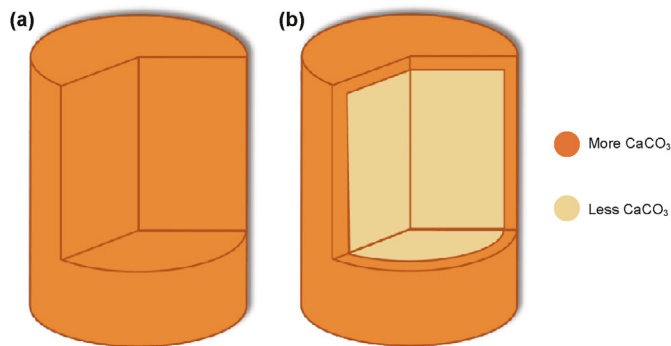


Fig. 11. Schematic of calcium carbonate distribution ((a) specimen of *Bacillus pasteurii*-CMC drilling fluid group; (b) specimen of *Bacillus pasteurii*-XG drilling fluid group).

0.024, and the greatest calcium carbonate production was 24.685 g. In contrast, of the 25 groups in the *Bacillus pasteurii*-XG drilling fluid experiment, 19 groups formed specimens with mechanical strength. The highest unconfined compressive strength here was 0.561 MPa, the lowest permeability coefficient 0.081, and the maximum calcium carbonate production 16.03 g. Li et al. (2022) investigated the MICP wall enhancing ability of undomesticated *Bacillus pasteurii* in CMC drilling fluids, and their results indicated that the specimens had the best performance with a maximum unconfined compressive strength of 0.324 MPa and calcium carbonate production of 6.31 g after 72 h of reaction at 0.6 mol/L cementing solution and an OD₆₀₀ value of 0.4 at room temperature. However, the specimens in this study exhibited better wall enhancing properties at higher temperatures and shorter reaction times, indicating that domestication significantly improves the growth activity of *Bacillus pasteurii* and its wall enhancing ability.

A comparative analysis of the orthogonal experimental results of *Bacillus pasteurii*-CMC and *Bacillus pasteurii*-XG drilling fluids

reveals superior performance parameters in the *Bacillus pasteurii*-CMC group under identical experimental conditions. This suggests more effective bacterial MICP curing in the *Bacillus pasteurii*-CMC drilling fluid.

The results of the unconfined compression experiment (Fig. 9) demonstrate that in the *Bacillus pasteurii*-CMC drilling fluid group, internal gravel soil particles are tightly bonded, maintaining a lump form post-fracturing with uniformly distributed mechanical strength, as shown in Fig. 11(a). In contrast, the *Bacillus pasteurii*-XG drilling fluid experiment resulted in specimens with only surface cementation and curing, forming a shell of certain mechanical strength. However, the internal particles remained loosely bound, leading to uneven mechanical strength distribution and overall lower strength, as depicted in Fig. 11(b). This difference is attributed to the larger molecular weight of XG compared to CMC (Yan, 2012), which enhances film-forming properties (Yang et al., 2017) but hinders *Bacillus pasteurii* infiltration into the specimen's interior. Consequently, minimal MICP reaction occurs inside the specimen, resulting in low mechanical strength. Conversely, in the *Bacillus pasteurii*-CMC group, the drilling fluid more effectively transports *Bacillus pasteurii*, Ca²⁺, urea, and nutrients into the specimen's interior, leading to a more uniform MICP reaction and higher mechanical strength as the fractured bodies are effectively cemented together.

3.2.1. Range analysis of *Bacillus pasteurii*-CMC drilling fluid groups

The experimental outcomes of the *Bacillus pasteurii*-CMC drilling fluid group, as derived from orthogonal experiments, have been analyzed using the range analysis method, as presented in Table 7.

Table 7 reveals that in the *Bacillus pasteurii*-CMC drilling fluid group, the factors influencing the unconfined compressive strength of the specimens are ranked as A > B > D > C. The optimal level combination for achieving the highest unconfined compressive strength is A₅B₄C₅D₅. For the permeability coefficient, the influencing factors are ranked as B > A > D > C, with the optimal combination being A₅B₄C₂D₅. Regarding calcium carbonate production, the order of influence is D > B > A > C, and the best level combinations for maximum calcium carbonate production are A₅B₅C₁D₅.

From Table 6, the optimal level combinations for unconfined compressive strength, permeability coefficient, and calcium carbonate production in the 25 groups of orthogonal experimental combinations are A₅B₅C₅D₅. Higher bacterial concentration and extended reaction time are beneficial, aligning with the range analysis results. However, the concentration of the cementing solution and temperature differ from the optimal combinations of the range analysis. This discrepancy can be understood by examining Fig. 12, which demonstrates that up to a 0.8 mol/L concentration, each performance parameter of the specimen improves as the cementing solution concentration increases. Beyond 0.8 mol/L, increased concentration only boosts calcium carbonate production, not strength or permeability reduction, corroborating findings from previous studies (Okwadha and Li, 2010; Al et al., 2012). Excessive calcium carbonate production near the specimen's surface hinders drilling fluid penetration and limits internal calcium carbonate generation. This results in uneven calcium carbonate distribution within the specimen, adversely affecting its overall performance. The range analysis indicates that temperature has the least impact on performance indices. The specimen exhibits the highest unconfined compressive strength, the second-lowest permeability coefficient, and the second-highest calcium carbonate production at the highest temperature condition of 45 °C. This suggests that induced and domesticated *Bacillus pasteurii* can effectively undergo the MICP reaction in higher-temperature drilling fluid

Table 7
Results of range analysis of specimens in *Bacillus pasteurii*-CMC drilling fluid group.

Performance indicator	Factor	Factor				Influence weight	optimal combination
		A	B	C	D		
Unconfined compressive strength	k_{i1}	0.326234629	0.339267	0.540507	0.447236	A > B > D > C	$A_5B_4C_5D_5$
	k_{i2}	0.56494846	0.55879	0.558379	0.472713		
	k_{i3}	0.654723732	0.701367	0.62662	0.570082		
	k_{i4}	0.659176849	0.733839	0.609375	0.751677		
	k_{i5}	0.796548876	0.668369	0.666752	0.759924		
	R_i	0.470314247	0.394572	0.126244	0.312688		
Permeability coefficient	k_{i1}	0.096752	0.105902	0.072005	0.085791	B > A > D > C	$A_5B_4C_2D_5$
	k_{i2}	0.068	0.064926	0.060983	0.082386		
	k_{i3}	0.063253	0.051939	0.072731	0.063351		
	k_{i4}	0.056801	0.046656	0.064507	0.059507		
	k_{i5}	0.04865	0.064035	0.06323	0.042422		
	R_i	0.048102	0.053963	0.011748	0.043369		
Calcium carbonate production	k_{i1}	7.431	6.476	14.789	6.428	D > B > A > C	$A_5B_5C_1D_5$
	k_{i2}	9.27	11.499	10.57	9.591		
	k_{i3}	12.018	10.149	8.74	11.164		
	k_{i4}	11.594	11.645	10.308	12.186		
	k_{i5}	14.739	15.283	10.645	15.683		
	R_i	7.308	8.807	6.049	9.255		

Note: k_{in} represents the average value of each performance index of the specimens in the *Bacillus pasteurii*-CMC drilling fluid group; $R_i = \max\{k_{in}\} - \min\{k_{in}\}$; $i = A, B, C, D$; $n = 1, 2, 3, 4, 5$.

environments, demonstrating good environmental adaptability. Nonetheless, the optimal combination still reflects improved activity of *Bacillus pasteurii* at suitable temperatures, highlighting the importance of enhancing the bacterium's environmental adaptability.

3.2.2. Range analysis of *Bacillus pasteurii*-XG drilling fluid groups

Similarly, the results of the *Bacillus pasteurii*-XG drilling fluid group, obtained from orthogonal experiments, have been scrutinized using the range analysis method. The corresponding data and analysis results are presented in Table 8.

Table 8 demonstrates that in the *Bacillus pasteurii*-XG drilling fluid group specimens, the factors influencing unconfined compressive strength are ranked as A > D > B > C, with the optimal combination for achieving the highest strength being $A_5B_4C_1D_5$. The permeability coefficient is similarly affected in the order of A > D > B > C, and the best combination for reducing permeability is $A_5B_3C_4D_5$. For calcium carbonate production, the order of impact is D > B > A > C, with $A_5B_5C_1D_5$ being the ideal combination for maximizing production.

Analysis of Table 6 and Fig. 13 shows that in the 25 orthogonal experimental combinations, the optimal level combinations for unconfined compressive strength, permeability coefficient, and calcium carbonate production are all $A_5B_5C_5D_5$. This indicates that higher bacterial concentration and longer reaction time enhance specimen performance, aligning with the range analysis results. However, cementing solution concentration and temperature diverge from the optimal combinations suggested by the range analysis. This implies that excessive cementing solution concentration, especially in the *Bacillus pasteurii*-CMC drilling fluid group due to XG's superior film-forming property, is detrimental. Similarly, excessively high temperatures negatively impact the MICP reaction.

In summary, the orthogonal experiments reveal that induced domesticated *Bacillus pasteurii* can effectively perform MICP in high-temperature drilling fluid environments. Higher initial bacterial concentrations and prolonged reaction times significantly improve specimen force performance, whereas overly high cementing solution concentration is counterproductive. Temperature has a relatively minor effect compared to the other factors. The

induced domesticated *Bacillus pasteurii* exhibits better adaptability to temperature in the *Bacillus pasteurii*-CMC drilling fluid group. This ensures that the *Bacillus pasteurii*-drilling fluid can better protect the borehole wall in the actual drilling process. In turn, it exhibits better borehole wall enhancing properties.

3.3. Microanalysis results

3.3.1. XRD analysis

Calcium carbonate exists in three primary crystal forms: calcite (rhombohedral hexahedral shape), aragonite (acicular), and vaterite (polycrystalline spherical shape). Of these, calcite is the most stable, aragonite is slightly less stable, and vaterite is the least stable (Almajed et al., 2018; Tirkolaei et al., 2020). To determine the predominant calcium carbonate types produced in each group, X-ray diffraction peak profiles of the specimens were compared and analyzed against standard diffraction peak profile PDF cards. The maps of the tested pure gravel soil sample, drilling fluid group, and *Bacillus pasteurii*-drilling fluid group are shown in Figs. 14 and 15, respectively.

Examination of Fig. 14 reveals an absence of discernible calcium carbonate wave peaks in the pure gravel soil sample and in both the CMC and XG drilling fluid groups. Predominantly, these specimens consist of quartz.

The XRD pattern of the *Bacillus pasteurii*-CMC drilling fluid group, as depicted in Fig. 15, reveals the presence of distinct calcium carbonate wave peaks in specimens from both the *Bacillus pasteurii*-CMC and *Bacillus pasteurii*-XG drilling fluid groups. In the *Bacillus pasteurii*-CMC drilling fluid group, the calcium carbonate crystals generated are identified as vaterite (CaCO_3), whereas in the *Bacillus pasteurii*-XG drilling fluid group, the crystals are calcite (CaCO_3). The XRD mapping analysis results demonstrate a notable contrast between the pure gravel soil samples, the drilling fluid group, and those treated with *Bacillus pasteurii*. The specimens subjected to *Bacillus pasteurii* drilling fluid exhibit characteristic diffraction peaks of spherical vaterite and calcite. This indicates the formation of calcium carbonate crystals of either vaterite or calcite type within these specimens.

This analysis suggests that the formation of calcium carbonate crystals plays a crucial role in the solidification and molding of

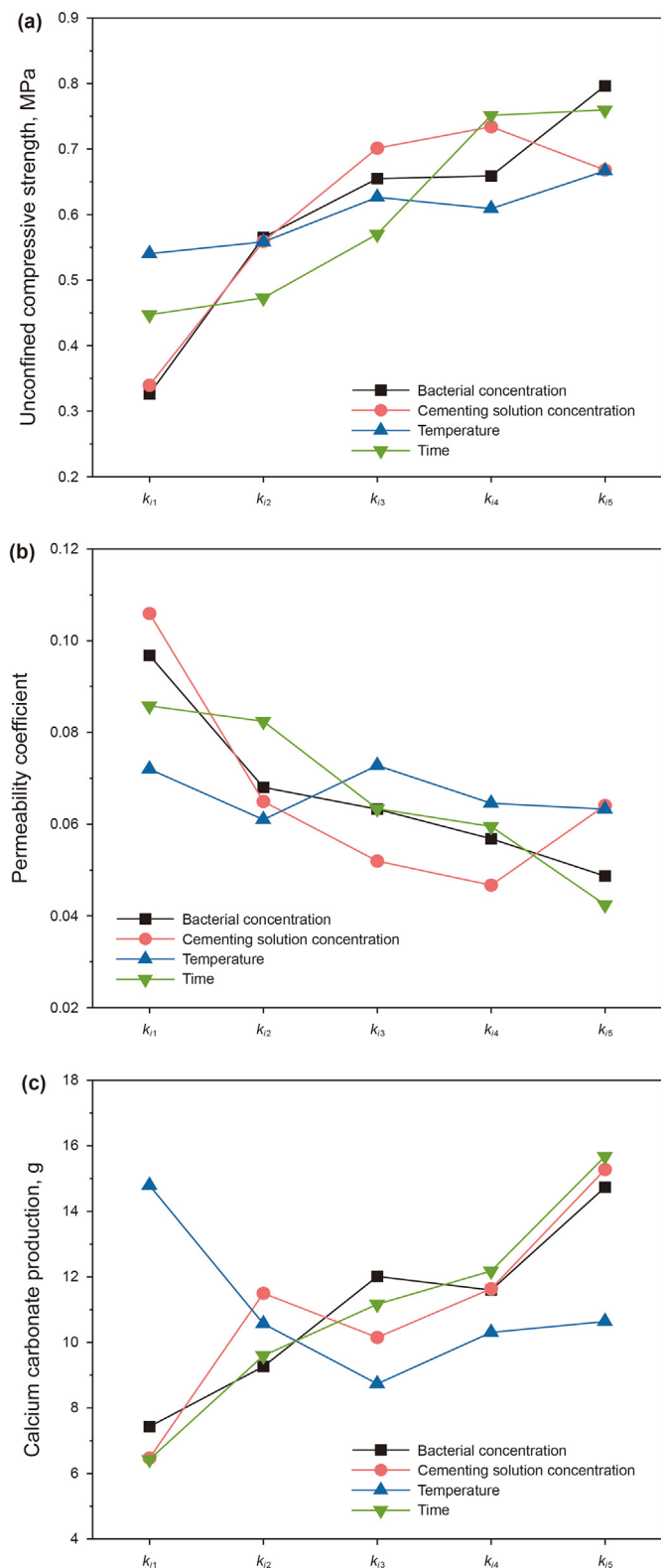


Fig. 12. Curve of the average value of each performance index of the specimen of *Bacillus pasteurii*-CMC drilling fluid group.

loose, uncemented gravel soil particles. It also appears to contribute significantly to the enhancement of mechanical properties and the reduction of the permeability coefficient. To delve deeper into the role of calcium carbonate crystals induced in the specimen by the

Bacillus pasteurii drilling fluid, and to confirm that the solidification and cementation of the specimen are indeed due to the generation of calcium carbonate, the microstructural changes of the specimen will be examined using SEM tests.

3.3.2. SEM analysis

Figs. 16 and 17 provide insights into the microscopic morphology of pure gravel soil sample, drilling fluid groups, and microbial drilling fluids.

In Fig. 16, no calcium carbonate crystals are observed on the surface of gravel soil particles from a pure gravel soil sample, drilling fluid P group, and drilling fluid Q group at 400 × magnification. This is why the specimens in the control group of the borehole wall enhancement experiment remained loose.

As shown in Fig. 17(a) and (b), the calcium carbonate crystals generated by MICP in *Bacillus pasteurii*-CMC drilling fluid are predominantly spherical crystals of varying sizes, indicative of vaterite type. At 400 × magnification, numerous vaterite crystals are uniformly attached to the surface of the gravel soil particles and fill the interstices. The particles exhibit a relatively flat surface, with vaterite crystals having a smaller diameter compared to gravel soil particles. At 1600 × magnification, these vaterite crystals are tightly interconnected, forming a dense “membrane” around the gravel soil particles, effectively cementing the loose particles together and greatly reducing pore space. The polymer, particularly sodium carboxymethyl cellulose in the solution, plays a crucial role in regulating calcium carbonate crystal morphology and selecting crystal type, favoring vaterite formation (Yang et al., 2013).

In Fig. 17(c) and (d), the calcium carbonate crystals generated by MICP in *Bacillus pasteurii*-XG drilling fluid are irregular polygonal crystals, indicative of calcite type. At 400 × magnification, numerous calcite crystals of varied sizes and distribution accumulate on the surface of the gravel soil particles, resulting in an uneven texture. At 1600 × magnification, these calcite crystals are densely packed, forming a “net” that tightly binds the particles together.

Comparing Fig. 16 with Fig. 17, gravel soil particles are observed to remain loose without the action of *Bacillus pasteurii* MICP. Conversely, after MICP wall enhancement experiments, numerous cemented calcium carbonate crystals form on the gravel soil particles' surfaces and in the interstices, improving particle cementation, shaping the gravel soil samples, and reducing interstitial space. This enhances mechanical strength and seepage resistance.

Comparing Fig. 17(b) and (d), the number of calcium carbonate crystals generated by the MICP reaction in *Bacillus pasteurii*-CMC drilling fluid is observed to be more abundant and evenly distributed. The cementation between these crystals and the gravel soil particles is tighter, resulting in less porous gravel soil particles and superior curing effects. This observation aligns with the results of unconfined compression and penetration experiments.

3.4. Analysis of the difference in wall enhancement performance of *Bacillus pasteurii* in different drilling fluids

Fig. 18 shows a schematic of the wall enhancement performance of different microbial drilling fluids.

During drilling into broken formations, *Bacillus pasteurii* is introduced into the borehole with the circulation of the drilling fluid. Due to the pressure differential between the formation pressure and the column pressure, *Bacillus pasteurii*, along with the drilling fluid, permeates into the surrounding formation. There, it distributes in the pore spaces or on particle surfaces, inducing the production of calcium carbonate crystals and exerting its wall enhancement effect. As drilling progresses and depth increases, the rising borehole temperature can inhibit the metabolic activity of

Table 8
Range analysis results of specimens in *Bacillus pasteurii*-XG drilling fluid group.

Performance indicator		Factor				Influence weight	Optimal combination
		A	B	C	D		
Unconfined compressive strength	k_{j1}	0.1241497	0.192914	0.360296	0.186774	A > D > B > C	A ₅ B ₄ C ₁ D ₅
	k_{j2}	0.2274336	0.289692	0.288689	0.16554		
	k_{j3}	0.3448668	0.33326	0.320097	0.311148		
	k_{j4}	0.3789693	0.390291	0.233693	0.41542		
	k_{j5}	0.4238995	0.293162	0.296544	0.420437		
	R_j	0.2997499	0.197377	0.126603	0.254897		
Permeability coefficient	k_{j1}	0.220099	0.225584	0.178154	0.216787	A > D > B > C	A ₅ B ₃ C ₄ D ₅
	k_{j2}	0.200414	0.188917	0.193166	0.210662		
	k_{j3}	0.182661	0.167058	0.198821	0.185353		
	k_{j4}	0.172565	0.167871	0.173212	0.161072		
	k_{j5}	0.145865	0.172173	0.178251	0.14773		
	R_j	0.074234	0.058527	0.02561	0.069057		
Calcium carbonate production	k_{j1}	4.718	4.345	11.215	3.98	D > B > A > C	A ₅ B ₅ C ₁ D ₅
	k_{j2}	7.246	7.63	6.922	7.642		
	k_{j3}	8.591	7.447	6.485	7.188		
	k_{j4}	7.621	8.27	6.174	8.909		
	k_{j5}	9.995	10.479	7.375	10.452		
	R_j	5.277	6.134	5.041	6.472		

Note: k_{jn} represents the average value of each performance index of the specimens in the *Bacillus pasteurii*-XG drilling fluid group; $R_j = \max\{k_{jn}\} - \min\{k_{jn}\}$; $j = A, B, C, D$; $n = 1, 2, 3, 4, 5$.

Bacillus pasteurii, potentially affecting its wall enhancement capabilities. However, *Bacillus pasteurii*, having undergone pH and temperature coupling gradient domestication, adapts to the increasing temperatures within the borehole, maintaining robust growth activity. It can produce a significant amount of urease in situ in granular pores or on particle surfaces, rapidly decomposing urea in the environment into NH_4^+ and CO_3^{2-} . Owing to *Bacillus pasteurii*'s cell wall structure, which is negatively charged, Ca^{2+} in the environment is adsorbed by the cells, inducing the formation of CaCO_3 crystals with the bacterium serving as a nucleation point, and enhancing cementation. However, differences in the cementation performance of *Bacillus pasteurii* in drilling fluids P and Q are observed. These variations are attributed to the differences in fluidity between the drilling fluids and the molecular weights of the polymers they contain, as well as the differing effects these polymers have on the formation of CaCO_3 crystalline phases (Chen et al., 2009). This may further amplify the disparities between the two fluids.

The number of hydroxyl and carboxyl groups present in the two polymers—CMC and XG—may be responsible for the differences in CaCO_3 crystallinity in drilling fluids P and Q (Wang et al., 2022). The strong electric field induced by the hydroxyl group exerts an attractive force on the nucleus, and this adsorption modifies the surface energy of vaterite, making it more thermodynamically stable than aragonite and calcite, which in turn affects the rate of spontaneous precipitation of vaterite and stabilizes it by preventing the transformation of vaterite to calcite (Flaten et al., 2009). In addition, Hu et al. (2010) suggested that carboxyl groups are also associated with promoting the generation and stabilization of vaterite-type CaCO_3 . They suggested the existence of coordination and electrostatic interactions between Ca^{2+} and carboxyl groups, and precipitation of Ca^{2+} and CO_3^{2-} in solution. The two actions occur competitively, in which the former negatively charged carboxyl groups can interact with some special interfacial molecular recognition between crystal surfaces to provide crystallization sites for CaCO_3 crystals. It means that the former can induce an increase in the local Ca^{2+} concentration, while further attracting CO_3^{2-} , increasing the local supersaturation degree, and promoting nucleation of crystals and heterogeneous nucleation and crystallization, which together provide the conditions for vaterite

generation.

Consequently, in the environment of drilling fluid P, the alkaline conditions and the presence of hydroxyl, carboxyl, and phosphate groups in *Bacillus pasteurii*, coupled with the abundance of hydroxyl and carboxyl groups in CMC, facilitate the formation and stabilization of the vaterite phase of CaCO_3 (Jiang et al., 2017). CMC, due to its smaller molecular weight, can penetrate deeper into smaller pore spaces, carrying increasing amounts of *Bacillus pasteurii* into the formation. The accumulating single crystals of spherical CaCO_3 interlock, filling the pore spaces and forming a dense, membrane-like structure that uniformly distributes between the fractured particles. This results in strong cementation, improving the strength of the broken formations, reducing their permeability, and thereby decreasing the likelihood of borehole wall destabilization.

Conversely, in the drilling fluid Q environment, the produced CaCO_3 crystals are predominantly in the calcite phase, as XG carries fewer hydroxyl and carboxyl groups, which is less conducive to the deposition and stabilization of CaCO_3 crystals in the vaterite phase (Flaten et al., 2009; Parakhonskiy et al., 2012). The hexahedral-shaped CaCO_3 crystals grow in clusters, forming a dense mesh in the shallower layers around the borehole wall. However, due to XG's large molecular weight and strong film-forming properties, which limit *Bacillus pasteurii*'s penetration depth, the distribution of calcium carbonate is relatively restricted and uneven, leading to less effective stabilization of the fracture body compared to the *Bacillus pasteurii*-CMC drilling fluid.

In conclusion, despite variations in wall enhancement performance across different drilling fluid environments, *Bacillus pasteurii*, when domesticated through pH and temperature coupling induction, demonstrates adaptability to high-temperature and strong alkali environments. It maintains robust growth activity under these conditions and can still efficiently induce calcium carbonate formation, which is advantageous for stabilizing borehole walls in broken formations. This result demonstrates the effect of inducing domestication and highlights the potential of the MICP technology in addressing borehole wall stability challenges in such environments. However, the current target temperature for the domestication of *Bacillus pasteurii* is only 45 °C, which can only be adapted to the temperature conditions of shallow holes. In the

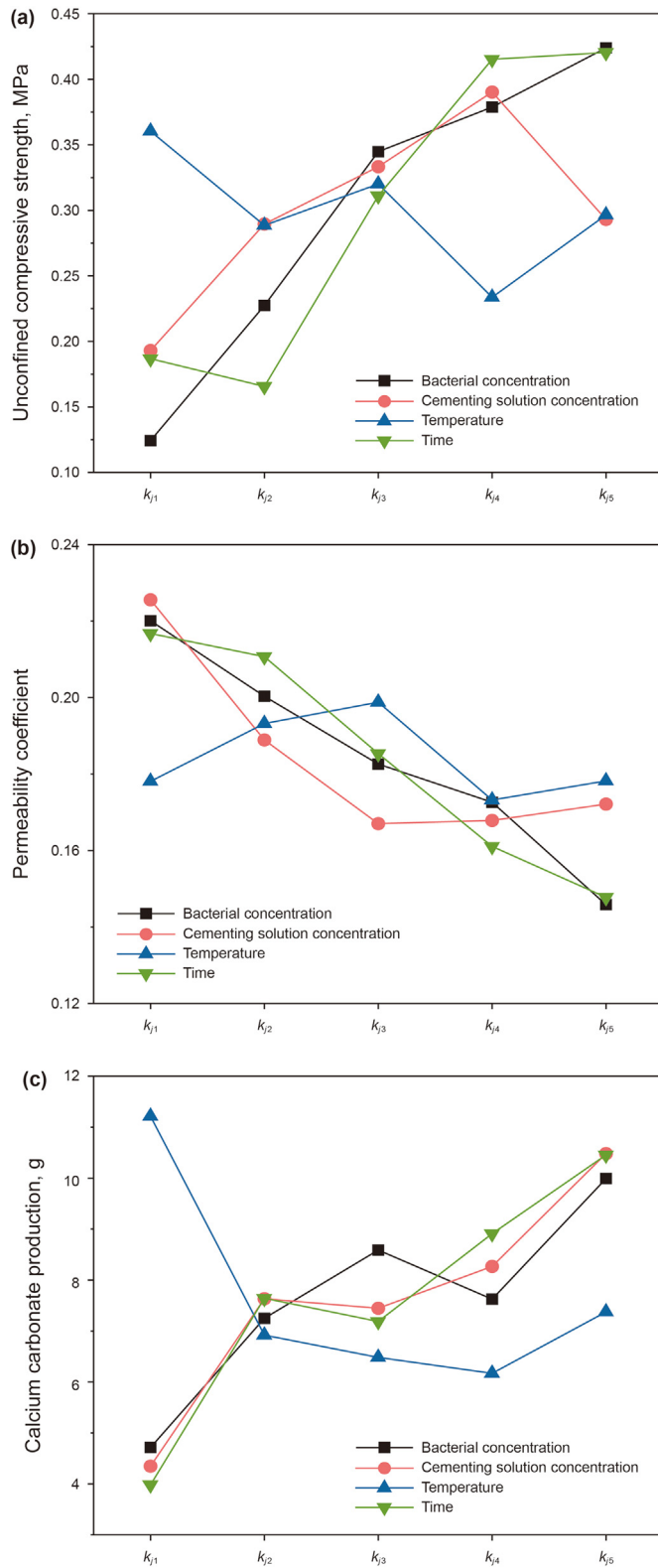


Fig. 13. Curve of the average value of each performance index of the specimen of *Bacillus pasteurii*-XG drilling fluid group.

future, the study of induced domestication under higher temperature conditions should be performed to improve the ability of *Bacillus pasteurii* to adapt to higher temperature environments to meet the needs of deep hole drilling.

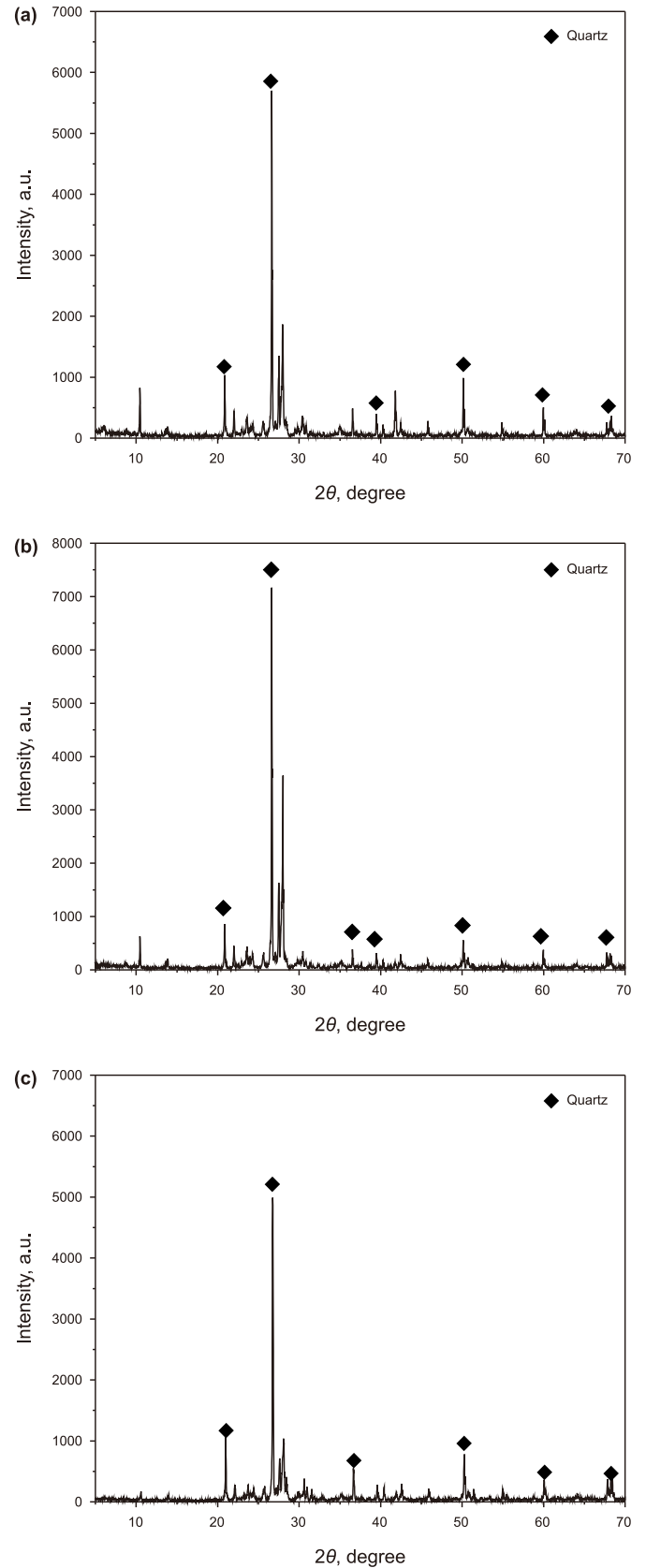


Fig. 14. XRD pattern of pure gravel soil sample, drilling fluid group ((a) pure gravel soil sample; (b) drilling fluid group P; (c) drilling fluid group Q).

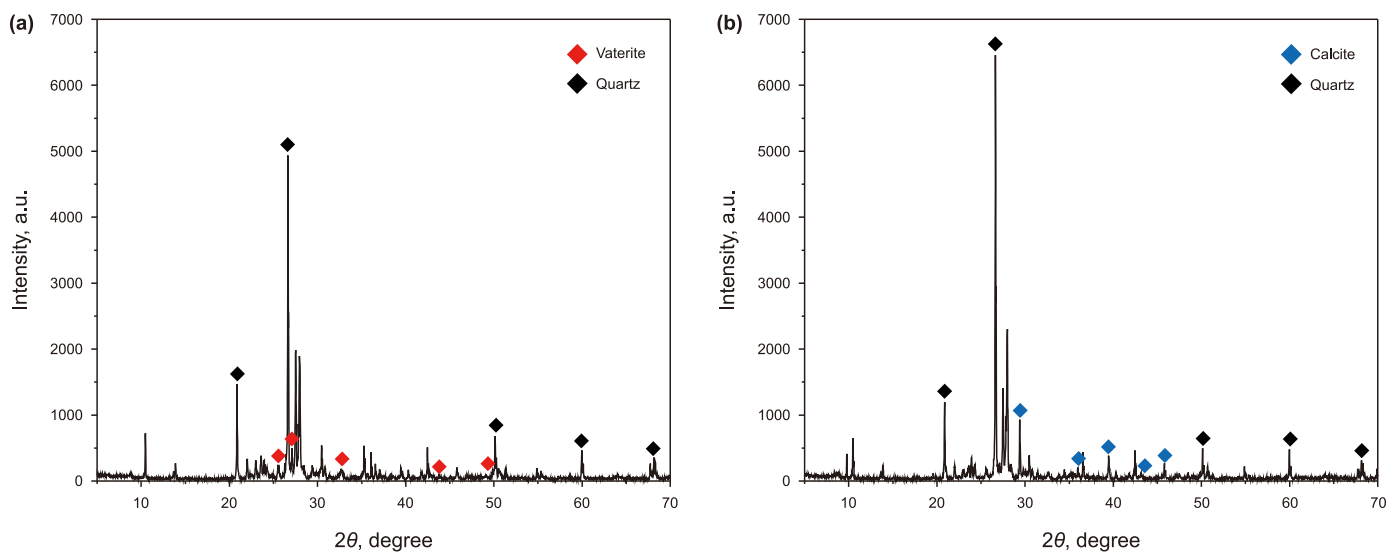


Fig. 15. XRD patterns of microbial drilling fluid groups ((a) *Bacillus pasteurii*-CMC drilling fluid group; (b) *Bacillus pasteurii*-XG drilling fluid group).

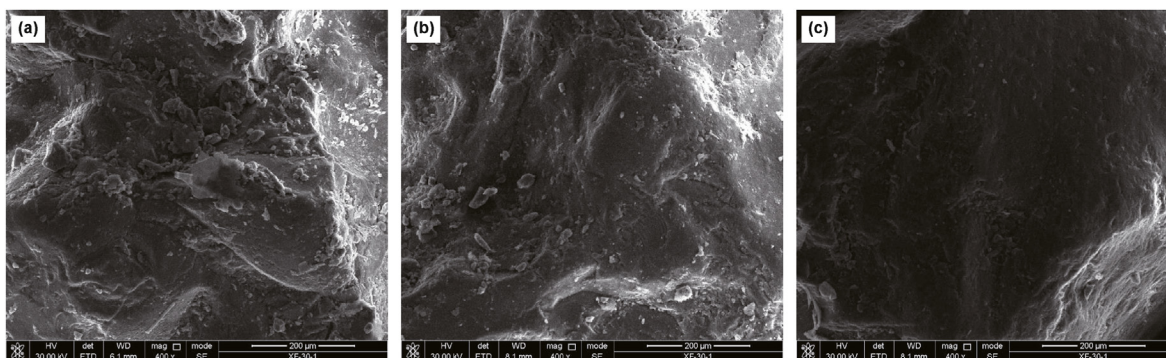


Fig. 16. Microstructural morphology of specimens of pure gravel soil sample and drilling fluid group ((a) pure gravel soil sample; (b) drilling fluid group P; (c) drilling fluid group Q).

4. Conclusions

In this study, a microbial drilling fluid system was established by integrating CMC, XG drilling fluids, and *Bacillus pasteurii*. The study employed both direct and gradient domestication schemes to achieve pH and temperature-coupled induced domestication of *Bacillus pasteurii* within the drilling fluid. The effectiveness and difference of the induced domesticated microbial drilling fluid on the borehole wall stabilization in broken formations was evaluated. The conclusions are as follows:

- (1) Through the process of pH and temperature coupled induced domestication, strains of *Bacillus pasteurii* capable of high growth activity at a pH of 10.3 and a temperature of 45 °C are obtained. Specifically, the bacterial concentration in the CMC drilling fluid is 1.373 with a urease activity of 1.98, while in the XG drilling fluid, the bacterial concentration is 0.931 with a urease activity of 1.76.
- (2) The results from orthogonal experiments on wall enhancement reveal that the higher the initial bacterial concentration, the longer the reaction time, the closer the temperature to the target temperature of domestication, and the higher

the concentration of cementing fluid but not more than 0.8 mol/L, the better is the borehole wall enhancement effect of MICP. Moreover, in the *Bacillus pasteurii*-CMC drilling fluid group, a larger quantity of calcium carbonate is produced, which is more evenly distributed and exhibits superior wall enhancement performance.

- (3) X-ray diffraction analysis and scanning electron microscopy tests indicate the induction of calcium carbonate in the specimens post wall enhancement experiment. In the *Bacillus pasteurii*-CMC drilling fluid, vaterite form of calcium carbonate crystals are induced. In the *Bacillus pasteurii*-XG drilling fluid, the induced calcium carbonate crystals are calcite.
- (4) During drilling in broken formations, the induced and domesticated *Bacillus pasteurii* can withstand increased pH and temperature in the borehole, inducing CaCO₃ crystals with the nucleation point on the bacterial body, increasing friction and cohesion between crushed particles, thereby improving the strength of the broken formations, reducing their permeability, and consequently enhancing the stability of the borehole wall.

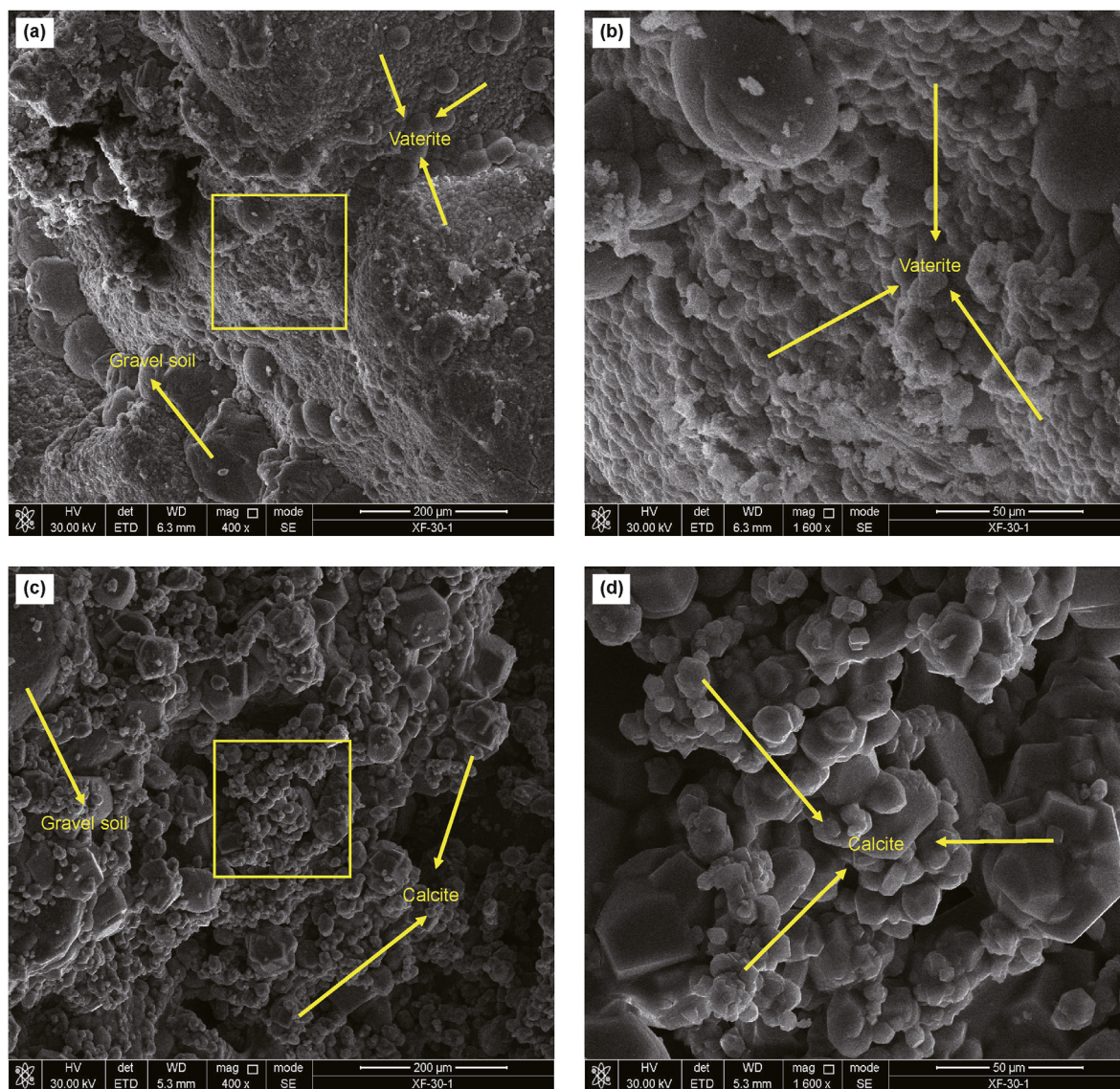


Fig. 17. Microstructural morphology of specimens from microbial drilling fluid groups ((a, b) *Bacillus pasteurii*-CMC drilling fluid group; (c, d) *Bacillus pasteurii*-XG drilling fluid group).

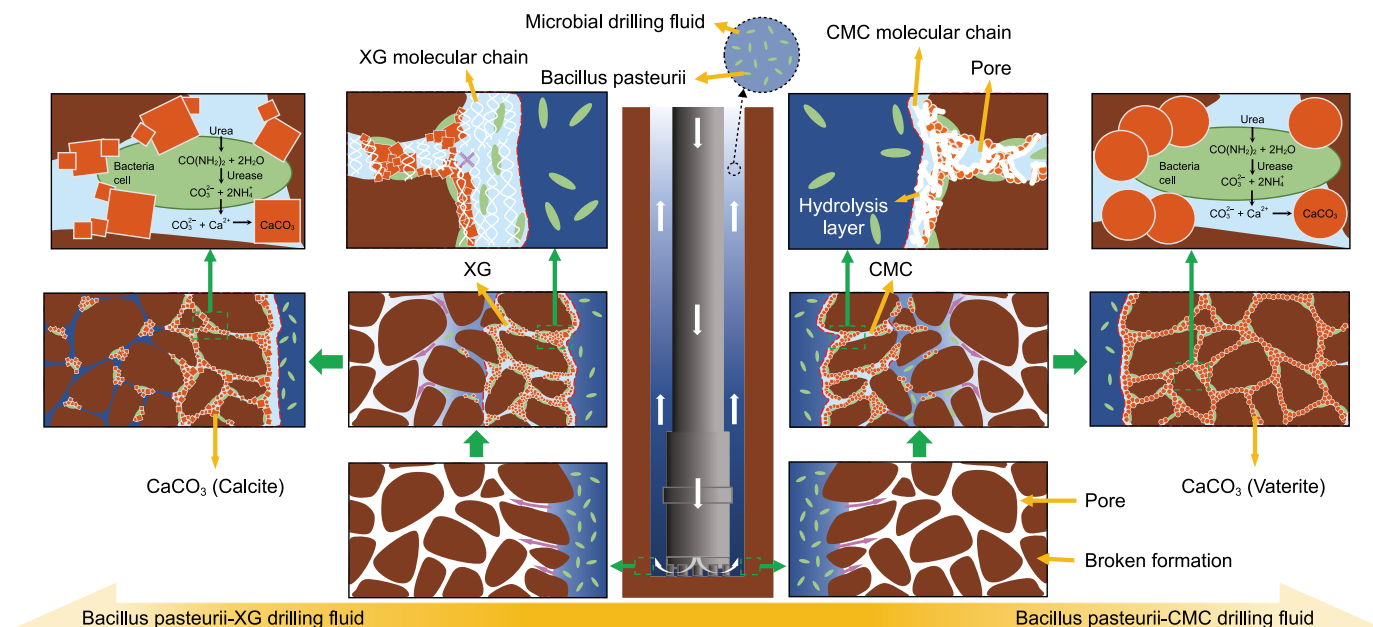


Fig. 18. Schematic of the wall enhancement performance of different microbial drilling fluids.

CRediT authorship contribution statement

Ze-Hua Du: Writing – original draft, Visualization, Validation, Investigation, Formal analysis, Data curation. **Zhi-Jun Li:** Writing – review & editing, Writing – original draft, Resources, Project administration, Methodology, Data curation, Conceptualization. **Jun-Xiu Chen:** Resources, Investigation, Formal analysis. **Zi-Yi Ma:** Validation, Resources. **Guang-Ding Guo:** Supervision. **Hao Zhang:** Supervision. **Sheng Wang:** Supervision.

Declaration of competing interest

The authors declare that they have no known competing financial interests or personal relationships that could have appeared to influence the work reported in this paper.

Acknowledgements

This study was supported by the State Key Laboratory of Geohazard Prevention and Geoenvironment Protection Independent Research Project (SKLGP2023Z012), the National Natural Science Foundation of China (Grant No. 41702388) and the Everest Technology Research Proposal of Chengdu University of Technology (Grant No.80000-2023ZF11411).

References

- Al, Qabany A., Soga, K., Santamarina, C., 2012. Factors affecting efficiency of microbially induced calcite precipitation. *J. Geotech. Geoenviron.* 138 (8), 992–1001. [https://doi.org/10.1061/\(asce\)gt.1943-5606.0000666](https://doi.org/10.1061/(asce)gt.1943-5606.0000666).
- Almajed, A., Tirkolaei, H.K., Kavazanjian, E., 2018. Baseline investigation on enzyme-induced calcium carbonate precipitation. *J. Geotech. Geoenviron.* 144 (11), 98–114. [https://doi.org/10.1061/\(asce\)gt.1943-5606.0001973](https://doi.org/10.1061/(asce)gt.1943-5606.0001973).
- Chen, Y.X., Zhao, G.Q., Wang, X.B., 2009. Control of the crystal polymorphs and morphology of calcium carbonate by polymers. *Prog. Chem.* 21 (22), 1619–1625 (in Chinese).
- Cui, Y.S., Feng, S.S., Huang, X., Chen, J.C., Yang, H.L., 2019. Directed domestication of Copper tolerance for enhancing lowgrade chalcopyrite bioleaching by *Acidithiobacillus caldus*. *Biotechnol. Bull.* 35 (8), 95–102. <https://doi.org/10.13560/j.cnki.biotech.bull.1985.2019-0103> (in Chinese).
- De Guidi, I., Legras, J.L., Galeote, V., Sicard, D., 2023. Yeast domestication in fermented food and beverages: past research and new avenues. *Curr. Opin. Food Sci.* 51. <https://doi.org/10.1016/j.cofs.2023.101032>.

- Flaten, E.M., Seiersten, M., Andreassen, J.P., 2009. Polymorphism and morphology of calcium carbonate precipitated in mixed solvents of ethylene glycol and water. *J. Cryst. Growth* 311 (13), 3533–3538. <https://doi.org/10.1016/j.jcrysgro.2009.04.014>.
- Fu, H.Y., Zhao, X.T., 2019. On the influencing factors of ground temperature gradient - taking Hu Xiang in Shangqiu area as an example. *Energy Environ.* 104–106. <https://doi.org/10.3969/j.issn.1672-9064.2019.04.048> (in Chinese).
- Harkes, M.P., van Paassen, L.A., Booster, J.L., Whiffin, V.S., van Loosdrecht, M.C.M., 2010. Fixation and distribution of bacterial activity in sand to induce carbonate precipitation for ground reinforcement. *Ecol. Eng.* 36 (2), 112–117. <https://doi.org/10.1016/j.ecoleng.2009.01.004>.
- He, Y.L., Sun, X.Y., Li, S.Y., Hao, D., 2023. High temperature acclimation and enzymatic properties of a lignin-degrading strain. *Microbiol. China.* 50 (1), 163–174. <https://doi.org/10.13344/j.microbiol.china.220403> (in Chinese).
- Hu, J.L., Tao, S.X., Ji, W.J., 2011. Borehole wall stability technology in broken formation and the practice. *Drill. Eng.* 38 (9), 30–32. <https://doi.org/10.3969/j.issn.1672-7428.2011.09.011> (in Chinese).
- Hu, Y.L., Ma, Y.J., Luo, Q.P., Zhou, Y., Pei, C.H., 2010. Laminated structure control of CaCO₃ micro-crystal by L-aspartic acid. *J. Synth. Cryst.* 39 (3), 802–806+812. <https://doi.org/10.16553/j.cnki.issn1000-985x.2010.03.015> (in Chinese).
- Ivanov, V., Chu, J., 2008. Applications of microorganisms to geotechnical engineering for bioclogging and biocementation of soil in situ. *Rev. Environ. Sci. Biotechnol.* 7 (2), 139–153. <https://doi.org/10.1007/s11557-007-9126-3>.
- Jiang, J.X., Wu, Y., He, Y., Gao, S., Zhang, C., Shen, T., Liu, J., 2017. Control of the crystal polymorphs and morphology of calcium carbonate by polymers. *Pro. Chem* 32 (7), 681–690. <https://doi.org/10.15541/jim20160484> (in Chinese).
- Kobayashi, H., Suzuki, T., Unemoto, T., 1986. Streptococcal cytoplasmic pH is regulated by changes in amount and activity of a proton-translocating ATPase. *J. Biol. Chem.* 261 (2), 627–630. [https://doi.org/10.1016/S0021-9258\(17\)36138-0](https://doi.org/10.1016/S0021-9258(17)36138-0).
- Krulwich, T.A., Sachs, G., Padan, E., 2011. Molecular aspects of bacterial pH sensing and homeostasis. *Nat. Rev. Microbiol.* 9 (5), 330–343. <https://doi.org/10.1038/nrmicro2549>.
- Li, Z.J., Chen, J.X., Zhao, G., Xiang, H.T., Liu, K., 2022. Effect and mechanism of microbial solid-free drilling fluid for borehole wall enhancement. *J. Pet. Sci. Eng.* 208 (PD). <https://doi.org/10.1016/j.petrol.2021.109705>.
- Li, Z.J., Huo, L.X., Zheng, J.Z., Zhang, S.X., Wu, X.K., 2023a. Growth kinetics of *Bacillus pasteurii* in Xanthan gum solid-free drilling fluid at different temperatures. *Geoenviron. Sci. Eng.* 223. <https://doi.org/10.1016/j.geoen.2023.211482>.
- Li, Z.J., Wu, X.K., Zhang, S.X., Du, Z.H., Ma, Z.Y., Tan, J.P., Li, Y.Y., 2023b. Growth kinetic model of *Bacillus pasteurii* under different pH and temperature conditions in sodium carboxymethyl cellulose solid-free drilling fluid. *Geoenviron. Sci. Eng.* 231. <https://doi.org/10.1016/j.geoen.2023.212372>.
- Li, Z.J., Zhao, G., Chen, J.X., Liu, K., Xiang, H.T., Tian, Y., 2021b. Growth kinetics of *Bacillus pasteurii* in solid-free drilling fluids. *ACS Omega* 6 (39), 25170–25178. <https://doi.org/10.1021/acsomega.1c02616>.
- Li, Z.J., Zhao, G., Xiang, H.T., Du, Z.H., Chen, J.X., Liu, K., 2021a. Preliminary study on wall enhancing and mechanism of microbe-CMC solid-free drilling fluid. Geological Society of China. In: Proceedings of the 21st Annual National Conference on Prospecting Engineering, Datong, Shanxi, China, pp. 261–265. <https://doi.org/10.26914/c.cnkihy.2021.022286> (in Chinese).

- Li, Z.Y., Liu, S.L., Reng, F.Z., Jin, J.H., Lu, D.X., 2016. Studies on fermentation performance domestication and its mechanism of *Lactobacillus paracasei* subsp. *paracasei* 9. *J. Chinese Inst. Food Sci. Technol.* 16 (7), 90–96. <https://doi.org/10.16429/j.1009-7848.2016.07.013> (in Chinese).
- Liu, D.M., Huang, J.J., Wang, R.L., Li, W., 2007. The factors affecting the pH of drilling fluids. *Oilfield Chem.* 91 (1), 1–4+29. <https://doi.org/10.19346/j.cnki.1000-4092.2007.01.001> (in Chinese).
- Liu, H.L., Xiao, P., Xiao, Y., Chu, J., 2019. State-of-the-art review of biogeotechnology and its engineering applications. *J. Civ. Environ. Eng.* 41 (1), 1–14. <https://doi.org/10.11835/j.issn.2096-6717.2019.001> (in Chinese).
- Niu, X.Y., Niu, X.J., Yin, B., Yang, A.H., 2012. Application of grouting and water plugging technology in soft and fractured strata. *Energy Technol. Manage.* (06) 54–56. <https://doi.org/10.3969/j.issn.1672-9943.2012.06.022> (in Chinese).
- Okwadha, G.D.O., Li, J., 2010. Optimum conditions for microbial carbonate precipitation. *Chemosphere* 81 (9), 1143–1148. <https://doi.org/10.1016/j.chemosphere.2010.09.066>.
- Parakhonskiy, B.V., Haase, A., Antolini, R., 2012. Sub-micrometer vaterite containers: synthesis, substance loading, and release. *Angew. Chem., Int. Ed.* 51 (5), 1195–1197. <https://doi.org/10.1002/anie.201104316>.
- Pei, D., Liu, Z.M., Hu, B.R., Wu, W.J., 2020. Progress on mineralization mechanism and application research of *Sporosarcina pasteurii*. *Prog. Biochem. Biophys.* 47 (6), 467–482. <https://doi.org/10.16476/j.pibb.2020.0012> (in Chinese).
- Phillips, A.J., Cunningham, A.B., Gerlach, R., Hiebert, R., Hwang, C.C., Lomans, B.P., Westrich, J., Mantilla, C., Kirksey, J., Esposito, R., Spangler, L., 2016. Fracture sealing with microbially-induced calcium carbonate precipitation: a field study. *Environ. Sci. Technol.* 50 (7), 4111–4117. <https://doi.org/10.1021/acs.est.5b05559>.
- Qi, H.Z., Ma, D.X., 2005. Analysis and practice of well wall stabilization in three-opening section of Tahe Oilfield. *Petrol. Drill. Tec.* 33 (1), 19–20. <https://doi.org/10.3969/j.issn.1001-0890.2005.01.006> (in Chinese).
- Qiu, Z.S., Li, J.Y., Shen, Z.H., 1999. A new method for evaluating the water sensitivity of mud shale-Specific hydrophilicity method. *Oil Drill. Prod. Technol.* 21, 1–6. <https://doi.org/10.13639/j.odpt.1999.02.001> (in Chinese).
- Steensels, J., Gallone, B., Voordeckers, K., Verstrepen, K.J., 2019. Domestication of industrial microbes. *Curr. Biol.* 29 (10), R381–R393. <https://doi.org/10.1016/j.cub.2019.04.025>.
- Sun, W.J., Yang, W.K., Li, J., Liu, R., Bai, J.J., Ren, X.Y., 2021. Darcy's experimental design in hydrogeology. *Sci. Tech. Inf.* 19 (5), 20–22+33. <https://doi.org/10.16661/j.cnki.1672-3791.2010-5042-1562> (in Chinese).
- Sun, X.H., Miao, L.C., Tong, T.Z., Wang, C.C., 2019a. Study of the effect of temperature on microbially induced carbonate precipitation. *Acta Geotech* 14 (3), 627–638. <https://doi.org/10.1007/s11440-018-0758-y>.
- Sun, X.H., Miao, L.C., Wu, L.Y., Chen, R.F., 2019b. Improvement of bio-cementation at low temperature based on *Bacillus megaterium*. *Appl. Microbiol. Biotechnol.* 103 (17), 7191–7202. <https://doi.org/10.1007/s00253-019-09986-7>.
- Tang, L., Luo, P.Y., 1997. Well wall stability analysis in fractured rock. *Oil Drill. Prod. Technol.* 19 (3), 1–5. <https://doi.org/10.13639/j.odpt.1997.03.001> (in Chinese).
- Tang, Y.M., Chen, J., Fu, X.B., Yang, F., 2012. Taming of the starter in soya-yogurt production. *Sci. Technol. Food Ind.* 33 (2), 185–188. <https://doi.org/10.13386/j.issn1002-0306.2012.02.064> (in Chinese).
- Tirkolaie, H.K., Javadi, N., Krishnan, V., Hamdan, N., Kavazanjian, E., 2020. Crude urease extract for biocementation. *J. Mater. Civ. Eng.* 32 (12), 1–12. [https://doi.org/10.1061/\(asce\)mt.1943-5533.0003466](https://doi.org/10.1061/(asce)mt.1943-5533.0003466).
- Wang, H.M., Wang, Y., Niu, M.H., Hu, L.H., Chen, L.B., 2022. Cold acclimation for enhancing the cold tolerance of zebrafish cells. *Front. Physiol.* 12, 813451. <https://doi.org/10.3389/fphys.2021.813451>.
- Wang, H.X., Miao, L.C., Sun, X.H., Wu, L.Y., Fan, G.C., Zhang, J.Z., 2023a. The use of N-(N-butyl)-thiophosphoric triamide to improve the efficiency of enzyme induced carbonate precipitation at high temperature. *Acta Geotech* 18 (9), 5063–5081. <https://doi.org/10.1007/s11440-023-01864-x>.
- Wang, H.X., Sun, X.H., Miao, L.C., Cao, Z.M., Guo, X., 2023b. Garlic extract addition for soil improvement at various temperatures using enzyme-induced carbonate precipitation (EICP) method. *J. Rock Mech. Geotech.* 15 (12), 3230–3243. <https://doi.org/10.1016/j.jrmge.2023.03.018>.
- Wang, L., 2017. Optimization and application of optimal support scheme for crushed soft rock roadway. *Mod. Min.* 33 (3), 202–203. <https://doi.org/10.3969/j.issn.1674-6082.2017.03.057> (in Chinese).
- Wang, X., Wei, M., Liu, K., 2022. Research progress on control and preparation of vaterite-type calcium carbonate. *Bull. Chinese Ceram. Soc.* 41 (8), 2860–2870+2878. <https://doi.org/10.16552/j.cnki.issn1001-1625.2022.08.013> (in Chinese).
- Wang, Y.H., Pan, Z.W., Zhang, J., Li, L.X., 2015. Law of permeability of porous continuous media and its extension. *J. Chifeng Univ.* 31 (7), 32–34. <https://doi.org/10.13398/j.cnki.issn1673-260x.2015.07.012> (in Chinese).
- Wang, Z.Y., 2022. Response Mechanisms to High Carbon during Photosynthetic Reactions of Microalgae with CO₂ Fixation from Flue Gas. Zhejiang University. <https://doi.org/10.27461/d.cnki.gzjdx.2022.001468> (in Chinese).
- Whiffin, V.S., 2004. Microbial CaCO₃ Precipitation for the Production of Biocement: PhD Dissertation. Murdoch University, Western Australia.
- Xiao, Y., Deng, H.F., Li, J.L., Cheng, L., Zhu, W.X., 2022. Study on the domestication of *Sporosarcina pasteurii* and strengthening effect of calcareous sand in seawater environment. *Rock Soil Mech.* 43 (2), 395–404. <https://doi.org/10.16285/j.rsm.2021.1455> (in Chinese).
- Yan, J.N., 2012. In: Dong, Ying (Ed.), *Drilling Fluid Technology (Revised Edition)*. China University of Petroleum Press, pp. 77–82 (in Chinese).
- Yang, S.C., Wang, Y.C., Pan, Y., Zhang, J.H., Zhao, H.Y., Luo, Y.D., 2017. Study and application of environmental friendly xanthan gum in petroleum exploitation. *Mod. Chem. Ind.* 37 (9), 40–43+45. <https://doi.org/10.16606/j.cnki.issn0253-4320.2017.09.009> (in Chinese).
- Yang, Y.N., Zhu, X.L., Kong, X.Z., 2013. Controls of crystal morphology, size and structure in spontaneous preparation of calcium carbonate. *J. Inorg. Mater.* 28 (12), 1313–1320. <https://doi.org/10.3724/SP.J.1077.2013.13163> (in Chinese).
- Zhang, J.C., Li, J., Xiao, P., Liu, H.L., Wu, H.R., 2023. Comparative study on MICP-treatment schemes for sands. *J. Civ. Environ. Eng.* 45 (6), 151–157. <https://doi.org/10.11835/j.issn.2096-6717.2022.125> (in Chinese).
- Zhang, S.H., Yu, C., Han, Y.F., Tang, Y., Shi, L.Y., Zhao, W., Wang, X.B., Zhang, X.X., Huang, Z.Y., Hu, L.Z., 2023. Research progress in microbial treatment of high-salinity industrial organic wastewater. *Microbiol. China.* 50 (4), 1720–1733. <https://doi.org/10.13344/j.microbiol.china.230081> (in Chinese).
- Zhang, W.J., He, Y., Wang, B., 2019. Adaptation mechanisms of microorganisms in extreme environment. *Agr. Jilin.* (16), 64–65. <https://doi.org/10.14025/j.cnki.jlmy.2019.16.037> (in Chinese).
- Zhang, Y.R., Zhang, Y.Z., Song, X.Y., 2022. Research progress in bioleaching of Copper ore. *Conserv. Util. Miner. Resour.* 42 (3), 125–134. <https://doi.org/10.13779/j.cnki.issn1001-0076.2022.07.003> (in Chinese).
- Zheng, X.F., Nie, Z.Y., Xia, J.L., Liu, L.Z., Yang, H.Y., 2019. Domestication of *Lep-tospirillum ferriphilum* arsenic-tolerant ability and mechanism of domestication. *Chin. J. Nonferrous Metals* 29 (3), 617–627. <https://doi.org/10.19476/j.ysxb.1004.0609.2019.03.21> (in Chinese).